

**Effective Thermal Conductivity Measurements Relevant to Deep
Borehole Nuclear Waste Disposal.**

By
Samina Shaikh
B.S/S.M Nuclear Science and Engineering

Submitted to the
Department of Nuclear Science and Engineering

In Partial Fulfillment for the Degree of
MASTER OF SCIENCE IN NUCLEAR SCIENCE AND ENGINEERING


At the
MASSACHUSETTS INSTITUTE OF TECHNOLOGY

January, 2007
[February 2007]

© 2007 Samina Shaikh. All rights reserved

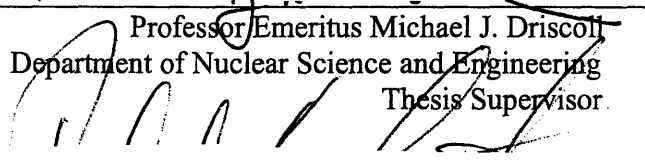
The author hereby grants to MIT permission to reproduce and distribute publicly
paper and electronic copies of this thesis document in whole or in part in any medium
now known or hereafter created

Signature of Author:



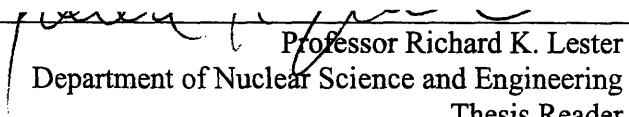
Department of Nuclear Science and Engineering
January 2007

Certified by:




Professor Emeritus Michael J. Driscoll
Department of Nuclear Science and Engineering
Thesis Supervisor

Certified by:

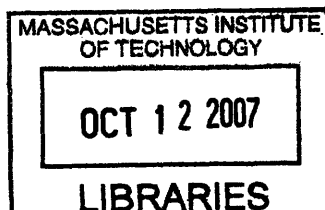


Professor Richard K. Lester
Department of Nuclear Science and Engineering
Thesis Reader

Accepted by:



Associate Professor Jeffery A. Coderre
Department of Nuclear Science and Engineering
Chairman, Committee for Graduate Students



ARCHIVES

Effective Thermal Conductivity Measurements Relevant to Deep Borehole Nuclear Waste Disposal.

By Samina Shaikh

Submitted to the Department of Nuclear Engineering on January 15th, 2006 in partial fulfillment of the requirements for the degree of Masters in Science in Nuclear Science and Engineering and Bachelors in Science in Nuclear Science and Engineering

Abstract

The objective of this work was to measure the effective thermal conductivity of a number of materials (particle beds, and fluids) proposed for use in and around canisters for disposal of high level nuclear waste in deep boreholes. This information is required to insure that waste temperatures will not exceed tolerable limits. Such experimental verification is essential because analytical models and empirical correlations can not accurately predict effective thermal conductivities for complex configurations of poorly characterized media, such as beds of irregular particles of mixed sizes.

The experimental apparatus consisted of a 2.54 cm. diameter cylindrical heater (heated length \approx 0.5 m) , surrounded by a 5.0 cm inner diameter steel tube. Six pairs of thermocouples were located axially on the inside of the heater sheath, and in grooves on the air-fan-cooled outer tube. Test media were used to fill the annular gap, and the temperature drop across the gap measured at several power levels covering the range of heat fluxes expected on a waste canister soon after emplacement.

Values of effective thermal conductivity were measured for air, water; particle beds of sand, SiC, graphite and aluminum; and an air gap subdivided by a thin metal sleeve insert. Results are compared to literature values and analytical models for conduction, convection and radiation. Agreement within a factor of 2 was common, and the results confirm the adequacy, and reduce the uncertainty of prior borehole system design calculations. All particle bed data fell between 0.3 and 0.5 W/m°C, hence other attributes can determine usage.

Thesis Supervisor: Professor Michael J. Driscoll
Title: Professor of Nuclear Science and Engineering

Acknowledgements

Despite the one author listed on the title page, no thesis work is the of a single individual, and this one is no exception. I express my sincere appreciation to my thesis advisor, Professor Michael J. Driscoll, for their guidance, never-ending patience and assistance from the initial selection of the research topic through the course of this investigation. I am also grateful for the use of the green lab and those responsible for running it, Gordon Kohse, Pete Stahle, Yakov Ostrovsky, and Tom Mckrell.

I also want to thank the Nuclear Regulatory Commission for funding my education at MIT and subsequent stay at the NRC.

Last but no means least, I would like to express a deep appreciation to my family: My mother, Sana and Samir. They deserve heartfelt thanks for their entire love and support.

Table of Contents

Abstract.....	2
Acknowledgements.....	3
Table of Contents.....	4
List of Tables.....	6
List of Figures.....	7
Chapter 1: Introduction.....	8
1.1 Background.....	8
1.2 Thesis Scope.....	9
1.3 Organization of this report.....	10
1.3.1 Deep Borehole Disposal Method.....	10
1.3.2 Analytical Considerations and Literature of Interest.....	10
1.3.3 Design of and Results from the Experiment.....	10
1.3.4 Discussion of Results.....	11
1.3.5 Recommended Future Work.....	11
Chapter 2: Deep Borehole Disposal Method.....	12
2.1 Introduction.....	12
2.2 Brief History of the Deep Borehole Waste Disposal Method.....	12
2.3 Disposal Burial Sites.....	13
2.4 Size and Depth.....	14
2.5 Decay Heat Removal.....	15
2.6 Chapter Summary.....	16
Chapter 3: Analytical Considerations and Literature of Interest.....	17
3.1 Introduction.....	17
3.2 Particle Size, Density and Thermal Conductivity.....	17
3.2.1 Other Models of Bed Conductivity.....	21
3.2.2 Other Models.....	23
3.3 Other Conductivity Measurements of Interest.....	26
3.4 Chapter Summary.....	27
Chapter 4: Design of and Results from the Experiment.....	28
4.1 Introduction.....	28
4.2 The Experimental Apparatus.....	28
4.2.1 Configuration for Current Experiments.....	32
4.3 Testing Conditions.....	40
4.4 The Experimental Program.....	42
4.4.1 Introduction.....	42
4.4.2 The Variables.....	43
4.5 Data	45
4.5.1 Overall Heat Transfer Coefficient.....	49
4.6 Chapter Summary.....	57
Chapter 5: Discussion of Results.....	59
5.1 Introduction.....	59
5.2 Overall Heat Transfer Coefficient Contribution.....	60

5.3 Overall Thermal Conductivity as a Function of Material Tested.....	64
5.4 Chapter Summary.....	66
Chapter 6: Future Work.....	67
6.1 Summary and Conclusions.....	67
6.2 Future Work.....	67
Appendix A: Calculations.....	68
A.1 Plots of axial temperature variation for different materials.....	68
A.2 Void space calculations of experimental particle beds.....	70
Appendix B: Description of Materials and Apparatus.....	71
B.1 Test Material Description.....	71
B.2 Apparatus Specification	74
Appendix C: Raw Data.....	77
References.....	106

List of Figures

Figure 2.1 Decay-heat power for spent fuel.....	16
Figure 3.1 Specification of Powder Beds.....	18
Figure 3.2 The Conductivity of Four UO ₂ Powder Beds in Helium As a Function of Temperature.....	19
Figure 3.3 Thermal conductivity of 500µm diameter sphere beds at a gas pressure of 0.1 MPa. Data points are experimental values.....	20
Fig 4.1 General Arrangement of Heater and Outer Pipe.....	30
Fig 4.2 Specific Features of Heater and Pipe Configuration.....	31
Fig 4.3 Fans Used to Cool Outer Cylinder of Heated Section.....	35
Fig 4.4 Picture showing Method of Vertical Suspension.....	33
Fig 4.5 Picture of Heated Length of Apparatus.....	34
Fig 4.6 Picture of Thermocouple Readout.....	36
Fig 4.7 Picture of Ammeter and Voltmeter.....	37
Fig 4.8 Experimental Setup: Overall Dimensions in mm.....	38
Fig 4.9 Typical Raw Data Set for a Run.....	45
Fig 4.10 Specific Thermocouple Locations Used for Data Analysis.....	46
Fig 4.5.1a Q vs. Delta T: Effective k for Air.....	50
Fig 4.5.1b Q vs. Delta T: Effective k for Silicon Carbide.....	51
Fig 4.5.1c Q vs. Delta T: Effective k for Graphite Sand.....	52
Fig 4.5.1d Q vs. Delta T: Effective k for Aluminum Powder.....	53
Fig 4.5.1e Q vs. Delta T: Effective k for Metal Sleeve.....	54
Fig 4.5.1f Q vs. Delta T: Effective k for Water.....	55
Fig 4.5.1g Q vs. Delta T: Effective k for Sand.....	56

List of Tables

Table 3.1 Literature Values of Thermal Conductivity of Materials of Interest.....	18
Table 4.1 Key Parameter for Test Rig.....	39
Table 4.2 Typical deep borehole and experimental setup data.....	40
Table 4.5.1a k and h Versus Power for Air.....	50
Table 4.5.1b k and h Versus Power for SiC.....	51
Table 4.5.1c k and h Versus Power for Graphite Sand.....	52
Table 4.5.1d k and h Versus Power for Aluminum Powder.....	53
Table 4.5.1e k and h Versus Power for Metal Sleeve.....	54
Table 4.5.1f k and h Versus Power for Water.....	55
Table 4.5.1g k and h Versus Power for Sand.....	56
Table 4.5.1h : average h and k as a function of material tested in annulus.....	57
Table 5.3.1 materials tested and their effective thermal conductivity.....	58

Chapter 1

Introduction

1.1 Background

One of the biggest obstacles facing the nuclear industry is what to do with spent nuclear fuel. Because it is highly radioactive and will remain so for many thousands of years, spent nuclear fuel is inherently dangerous to human health, now and for future generations. Because it contains materials used in making nuclear weapons, spent fuel also poses proliferation risks.

Most countries' preferred option for isolating spent fuel from humans and the environment is to bury it underground in a deep geological repository. In the United States, which has a repository schedule decades ahead of other countries, Yucca Mountain (YM) is being developed by the Department of Energy as the sole solution for the disposal of spent fuel. Proponents want it to be the country's first underground storage facility for spent fuel from the 100-plus commercial nuclear power plants in the United States [1]. But Yucca may not be the sole solution to the nuclear waste problem. This circumstance is in part due to the recently initiated GNEP program, which envisions separation of the waste into several streams to tailor disposal methods to the best available approach. The geology of Yucca Mountain, volcanic tuff, may not provide a verifiably impervious barrier in the very long term [2]. Also, serious questions have been raised about the integrity of the canisters that would hold the spent fuel [2]. U.S. Department of Energy (DOE) assessments assume that the engineered barriers, notably the metal canisters, will provide adequate containment. A potentially better alternative is the deep borehole strategy. In this disposal option, the waste is emplaced in a several

kilometers deep geologic borehole of the type currently drilled for oil, gas and geothermal applications, under suitable engineering and geological conditions preferably into high integrity granite rock [3]. In contrast to YM, boreholes will rely on the geology as the main barrier to radiological waste transport. It is predicted that boreholes will effect a dramatic reduction in the amount and prolongation of the time scale, of waste escape, at acceptable project costs, and with better prospects for public/political acceptance. The major uncertainty with this option is the waste form temperature in situ. This study will address this question and focus on the effective thermal conductivity of materials proposed for use in and around canisters for deep borehole waste disposal.

1.2 Thesis Scope

This thesis deals with the design and use of an experimental simulation of a deep borehole waste disposal system, to measure temperature in-situ. In a deep borehole system spent fuel rods are placed in a canister and entombed in a cylindrical hole bored into granite rocks. Different media will be present between the heat source (i.e spent fuel) and host rock. The temperature difference between heat source and rock will be determined by the effective thermal conductivity of this intervening material.

Determining the effective thermal conductivity, the subject of the experiment, will help determine which composition will be best suited for waste canister design and the canister/borehole interface.

This research will investigate the thermal conductivity of several different materials such as air, water, sand, silicon carbide, and graphite. These thermal conductivities will help assess the best mixture in providing an efficient decay heat removal means.

1.3 Organization of this report

This thesis will have five sections:

1.3.1 Deep Borehole Disposal Method

Before discussing experimental design, background information on deep borehole method must be discussed. Chapter 2 discusses the history of deep borehole approach and the hole size and rock type deep boreholes are best suited for. And finally this chapter will also discuss the key heat removal processes associated with this disposal method.

1.3.2 Analytical Considerations and Literature of Interest

Chapter 3 is a detailed analysis of different heat transfer models that will be applicable to our experiments. Much of the work discussed will revolve around particle size and its relation to the conductivity of particle beds.

1.3.3 Design of and Results from the Experiment

This chapter deals with the experimental setup and the hardware used in the experimental runs. Also, descriptions of the experimental program, measured variables, experimental conditions, concluding with measured data, will be presented.

1.3.4 Discussion of Results

The main focus of this thesis is to determine experimentally, overall heat transfer coefficients under different operational conditions. Also discussed, is what the data will mean to deep borehole waste disposal.

1.3.5 Recommended Future Work

Chapter 5 will discuss any other experimental conditions that may be investigated to better understand the heat transfer problem. One such issue is filling any gaps with concrete or grout and its effect on the effective thermal conductivity. Another innovation would be filling the canister with sand and a fill gas of helium.

Chapter 2

Deep Borehole Disposal Method

2.1 Introduction

This chapter will present a historic review of the deep borehole waste disposal method. The purpose is to provide enough technical detail to understand the design of the deep borehole experiment, which will be explained in greater detail in Chapter 3.

2.2 Brief History of The Deep Borehole Approach [1] [2] [4]

In this method of high level radioactive waste disposal, solid packaged wastes are placed in deep boreholes drilled to depths of several kilometers, with diameters of typically less than one meter. The waste containers are stacked in each borehole and could be separated from each other by a layer of bentonite or cement. The top two kilometers would be sealed with materials such as bentonite, asphalt or concrete. The US, UK, Sweden, Finland and Russia, among others, have examined the deep borehole method as a possible alternative to a shallow mined repository. Boreholes could be drilled both offshore and onshore in many types of rock, which broadens the number of possible disposal sites. Although proponents argue that related long-term risks to people and the environment would be very low, there are significant technical questions requiring further research.

In the oil industry boreholes are readily drilled offshore as well as onshore, through unstable rock units, and can deal with high pressure fluids and can penetrate to depths of

more than 10 km. This capability to drill to great depths significantly expands the range of locations that could be considered for radioactive waste disposal and could include geological settings which might have advantages in terms of environmental effects or long-term safety over those suitable for a mined repository.

This section reviews the deep borehole disposal concept to the present day. As a concept, it has always been subsidiary to the more conventional mined geological repository and, although it has been considered in several different countries for the disposal of long-lived waste, sometimes over many years, it has never been selected as the preferred option for disposal. During the 1990s the concept was investigated for the disposal of excess weapons-grade plutonium and more recently it has been considered in a variety of versions, including the disposal of heat-emitting waste in schemes which involve the melting or partially melting of the host rock. Its most promising use may be for countries which have only small volumes of waste for disposal and where such a concept might prove more suitable than the construction of a mined repository.

2.3 Disposal Burial sites

Rock Type

Igneous (Granite)

Igneous rock masses, particularly granite have been the favored rock type for HWL repository designs, having great rock strength, low porosity and high thermal conductivity. High-temperature, high-pressure experiments show that granite can be partially melted and completely recrystallized on a time scale of years as opposed to

millennia as widely believed. This could prove the key to secure, very deep borehole disposal in the continental crust for small to moderate volumes of particularly problematic radionuclides. The recrystallization process will help seal any faults or cracks which, though not detrimental at these depths, may provide quicker transport pathways. Removal of these problematic isotopes from spent nuclear fuel and other forms of high-level waste could open the way to safe and acceptable disposal of the remaining bulk of high-level waste with large volumes of intermediate-level waste in geologically shallow, conventional repositories.

Statistically 95 % of the Earth's crust is igneous. Since 75% of the surface is sedimentary with an average depth of 2 km this suggests that mostly anywhere in the United States you will find igneous rock 2 km underground. There are known surface expressions in Canada around Hudson Bay which suggest that there is a gradual rise toward the surface of subsurface granite in the northern United States; possibly suggesting a smaller sedimentary layer in this area.

2.4 Size and Depth

As stated above, the holes are expected to go down to about 4 km underground. This number is a loose function of the economic feasibility of deep drilling, rock type location, heat, and pressure. No matter the depth, the filling of the holes is limited to about 1 km of waste due to the weight of the packages. Higher packing may cause the bottom canisters to rupture under the loading. Though boreholes do not rely on the integrity of these canisters they are still another measure of containment, and contribute

to public acceptance. Therefore we can assume depth and pack length are set factors. The size specification up for decision is the diameter of the hole.

Current designs recommend around a 0.6 meter hole diameter. This is dependent on the drilling technology, the stability of the hole, and economics. This 0.6 meter hole is usually cited in conjunction with a vertical 1 km waste stack length. A larger diameter hole would give room for more fuel storage, but increasing the diameter would increase the heat flux which could lead to cracking in the rocks or melting of the canisters.

It is also of current economic significance that 12 in (30.5 cm) boreholes are the oil industry standard. Though 60 cm holes are achievable, it is with increased cost.

Most likely the canister would be made of strong steel with a copper outer shell to prevent corrosion by the brine contained in the rock. Each canister is 5 meters tall and contains one PWR assembly in a 60 cm hole. Hence one kilometer of these stacks of canisters contains 200 assemblies, each containing about 500kg of heavy metal. It is therefore estimated that each hole would contain about 100 MT.

2.5 Decay Heat Removal

A concern regarding deep borehole waste disposal is the waste material's temperature. If the waste material is hot enough, it can possibly melt the host rock or perhaps cause the host rock to crack. PWR fuel assemblies in the US, which are about four meters tall, have an average burnup between 18 and 40 GWd/MTU for assemblies with at least ten years of cooling [4]. Fig 2.4 is a representative decay heat profile of spent nuclear fuel. Limits regarding waste and storage have been quoted by Manteufel

[17]. However these are not necessarily definitive limits. Hoag has calculated temperatures suitable for granite host rock disposal, however these are only analytical and have not been confirmed by experimentation.

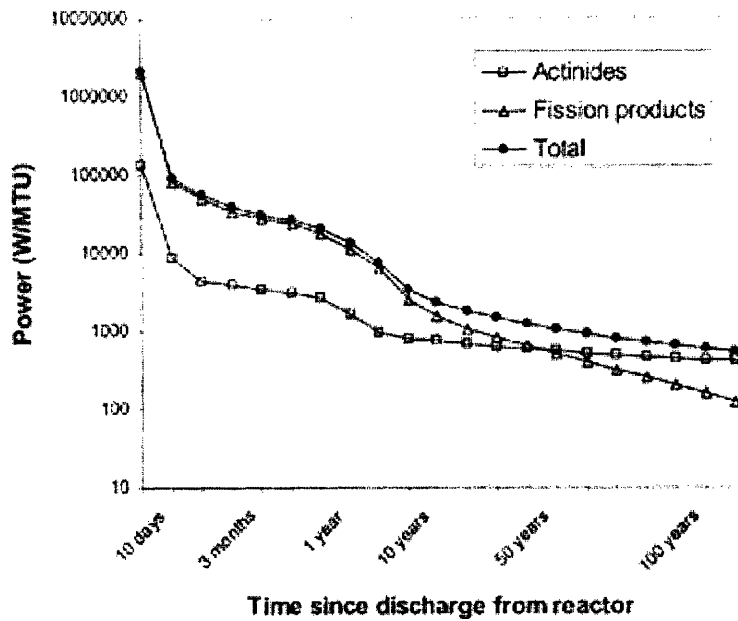


Fig 2.1 Decay-heat power for spent fuel (measured in watts per metric ton of uranium) plotted on a logarithmic scale as a function of time after reactor discharge. [5]

2.6 Chapter Summary

This chapter presents the historical overview of the deep borehole waste disposal method, as well as other technical information, such as, rock type employed for waste disposal, size and depth of disposal site, and finally the decay heat removal requirements.

Chapter 3

Analytical Considerations and Literature of Interest

3.1 Introduction

In this chapter we will discuss analytical work done by others to determine thermal conductivities of material that may be relevant for deep borehole experimentation: beds of particles in particular. Much of the work discussed will revolve around particle size and its relation to the conductivity of particle beds. Analytical models used to interpret our experimental data will be discussed in chapter 5

3.2 Particle Size, Density and Thermal Conductivity

Considerable work has been done over the past several decades on compacted particle beds for use as nuclear fuel. Such work is directly applicable here. Reference [6] presents thermal conductivity measurements on four different UO_2 powder beds. These are a coarse, fine, two-fraction bed and a three-fraction bed; the latter to achieve high density by using different particle sizes for each fraction. Figure 3.1 list the particle beds tested and 3.2 shows the results of this study [6]. At each temperature the coarse particle beds consistently have higher conductivity than the fine particle bed, and the high smear density beds have higher conductivity than those of lower density. Figure 3.3 shows the strong effect of fill gas conductivity [18].

This prior work can help evaluate the magnitude and trends of the results of the conductivity measurements carried out in the present work. It is also noteworthy that the authors of reference [7] employed an apparatus very similar in design to the one used in the present work.

Bed	Composition by weight	Packing fraction	Smear density
Coarse	100% coarse	0.625	0.616
Fine	100% fine	0.593	0.585
Two-fraction	55% coarse + 45% fine	0.810	0.799
Three-fraction	59% coarse + 20% medium + 21% fine	0.877	0.866

Fig 3.1 Specification of Powder Beds Tested in Reference [6]¹

¹ Coarse sand as regarded as having effective diameters between 2.0 and 0.2mm, and for fine sand the range is between 0.2 and 0.02mm.



Fig 3.2 The Conductivity of Four UO₂ Powder Beds in Helium As a Function of Temperature Ref [6]

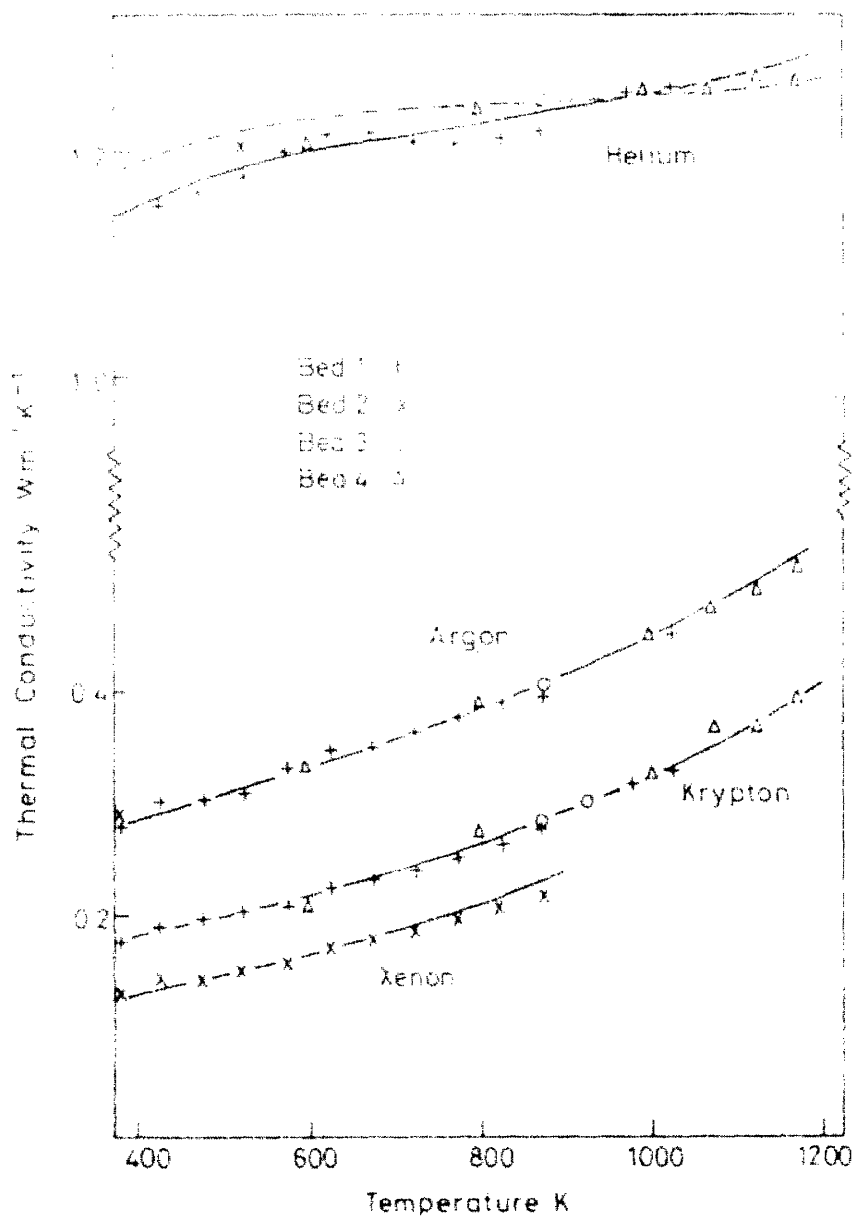


Fig 3.3 Thermal conductivity of 500µm diameter sphere beds at a gas pressure of 0.1 MPa. Data points are experimental values.

3.2.1 Other Models of Bed Conductivity

Below are several models developed by the authors noted for estimating conductivity. Specific numerical examples of a SiC bed and air filled gaps are also calculated .

Batchelor's model [7] gives this simple correlation:

$$k_{bed}/k_g = 4 \ln (k_p/k_g) - 11 \quad \text{eqn. 3-1}$$

Where k_p = thermal conductivity of particle material, for example SiC ~ 42 W/m°C

k_g = thermal conductivity of fill gas, ex. Air= 0.03 W/m°C

This predicts $k_{bed} = 0.54$ W/m°C. This model is oversimplified and does not take into account particle shape, void fraction, or interface resistance between bed and container wall. Moreover this model was developed for uniformly sized particles and will not be suitable in modeling commercial grade SiC, which is neither pure nor uniform.

Kunii and Smith [8]

Cubic array sphere

$$k_{bed}/k_g = (0.7845) (2) (k_p/(k_p-k_g))^2 (\ln (k_p/k_g) - (k_p-k_g/k_p) + 0.2146) \quad \text{eqn. 3-2}$$

$k_g = 0.03$ W/m°C

k_p = Thermal conductivity of particle material, for example SiC ~ 42 W/m°C

$$k_{bed} = 0.301 \text{ W/m}^\circ\text{C}$$

Orthonormal spheres

$$k_{bed}/k_g = (0.9069) (2) (k_p/(k_p-k_g))^2 (\ln(k_p/k_g) - (k_p-k_g)/k_p) + 0.0931 \quad \text{eqn. 3-3}$$

With k_g and k_p values as above

$$k_{bed} = 0.343 \text{ W/m}^\circ\text{C}$$

Krupiczka [8]

Spherical lattice spheres

$$\log(k_{bed}/k_g) = (0.7854 - 0.057 (\log(k_p/k_g))) * \log(k_p/k_g) \quad \text{eqn. 3-4}$$

$$k_{bed} = 0.444 \text{ W/m}^\circ\text{C}$$

Mohamad [8]

$$k_{bed} = (2 k_g / 1 - k_p / k_g) [(\ln(k_p / k_g) / (1 - (k_g / k_p))) - 1] \quad \text{eqn. 3-5}$$

$$k_{bed} = 0.495 \text{ W/m}^\circ\text{C}$$

Thus depending on the model employed, values of effective bed conductivity can vary by nearly a factor of 2 due to modeling inconsistencies.

3.2.2 Other Models

Mikheyev's correlation for convection [9]:

$$k_{\text{eff}} / k = A * \delta (\Delta T / \delta) \quad \text{eqn. 3-6}$$

In which

k = thermal conductivity of fluid

δ = distance between planes

$$\text{Where} \quad A = 0.18 (g B Pr / v^2)^{1/4} \quad \text{eqn. 3-7}$$

In which

B = Thermal expansion coefficient $1/^\circ\text{C}$

g = m/sec^2

v = viscosity $\sqrt{[\text{m}/\text{sec}]}$

Pr = Prandtl number, dimensionless

For air $A = 18.9 - 0.048 T \text{ } ^\circ\text{C}$ $10 \leq T \text{ } ^\circ\text{C} \leq 150 \text{ } ^\circ\text{C}$

For water $A = 56.7 - 0.54 T \text{ } ^\circ\text{C}$ $17 \leq T \text{ } ^\circ\text{C} \leq 95 \text{ } ^\circ\text{C}$

Example for air:

Let $\delta = 1.3 * 10^{-2} \text{ m}$, $\Delta T = 50 \text{ } ^\circ\text{C}$ $T = 65 \text{ } ^\circ\text{C}$

Then $A = 15.78$

$k_{\text{eff}} / k = (15.78) (1.3 * 10^{-2} \text{ m}) (5000)^{1/4} = 1.73$

If $k_{air} = 0.03 \text{ W/m}^\circ\text{C}$, $k_{eff} = 0.052 \text{ W/m}^\circ\text{C}$, an order of magnitude less than representative particle bed powder.

To which we need to add $k_{radiation}$

Example for water:

Let $\delta = 1.3 \cdot 10^{-2} \text{ m}$, $\Delta T = 10 \text{ }^\circ\text{C}$ $T = 50 \text{ }^\circ\text{C}$

Then $A = 83.7$

$k_{eff} / k = (83.7) (1.3 \cdot 10^{-2} \text{ m}) (1000)^{1/4} = 6.12$

If $k_{water} = 0.6 \text{ W/m}^\circ\text{C}$, $k_{eff} = 3.67 \text{ W/m}^\circ\text{C}$

Note the large improvement with water.

Effective Thermal Conductivity Due to Radiation [10]

$$k_{radiation} = 4\sigma \delta T^3 [1 + 1/4 (\Delta T/T)^2] \quad \text{eqn. 3-8}$$

Where $\sigma = \text{Stefan- Boltzman constant} = 5.67 \cdot 10^{-8} \text{ W/m}^2 \cdot \text{K}^4$

$\delta = \text{distance between planes}$

Example for air:

Let $\delta = 1.3 \cdot 10^{-2} \text{ m}$, $\Delta T = 50 \text{ }^\circ\text{C} + 273 \text{ }^\circ\text{K}$ $T = 65 \text{ }^\circ\text{C} + 273 \text{ }^\circ\text{K}$

Then $k_{radiation} = 0.122 \text{ W/m}^\circ\text{K}$

Note that this is three times the value for convection.

Effective Thermal Conductivity[10]

We will require an expression relating measurable values to the effective conductivity of material in an annulus gap, as follows:

$$k = \frac{(Q/L) * \ln (R_2/R_1)}{(2\pi \Delta T)} \quad \text{eqn. 3-9}$$

Q = heater power, watts

L = Active length of heater (0.457m)

ΔT = mean temperature difference across gap

$R_2/R_1 = D_2/D_1$ = ratio of shell inner diameter to heater outer diameter

Example:

Let Q = 20 W , ΔT =50 °C, $R_2/R_1 = 2$

k = 0.096 W/m°C

3.3 Other Conductivity Measurements of Interest

Table 3.1 is a summary of various measurements or calculations made to determine thermal conductivities collected from a literature survey.

Table 3.1 Literature Values of Thermal Conductivity of Materials of Interest

Material	K, W/m ^o K	Reference	Comment
Solids			
Granite	1.73- 3.98/3.4	McAdams[11]	
Cement	1.3/0.9/ 0.92/ 1.7	McAdams [11]/ Dean's Handbook[12]/ CRC [13]	
Liquids			
Water	0.65	Dean's Hand book [12]	
Air	0.03	CRC[13]	
Particle Bed			
Sand	0.33/0.39	McAdams[11]/ Dean's Handbook[12]	
SiC	0.33	Kao[14]	
Graphite powder	0.18	McAdams [11]	100 mesh powder

3.4 Chapter Summary

The strong effect of parameters such as particle size, shape, size distribution (which determines contact area and packing density) make measurements essential, since analytical models are incomplete, and the requisite characterization parameter will be lacking for materials of interest. In the next two chapters experimental data will be acquired to provide verified pertinent effective thermal conductivity data for use in future deep borehole system design.

Chapter 4

Design of and Results from the Experiment

4.1 Introduction

This chapter starts with a description of the hardware and experimental setup used in the experimental runs. The apparatus used is a modification of the one by Novak and Marques [15] [16]. In addition, the chapter presents a discussion of the experimental program describing measured variables, the experimental conditions and the operational procedures, concluding with documentation of measured data.

4.2 The Experimental Apparatus

The experimental apparatus is an alteration of the device originally constructed by Novak [15], as part of his MS thesis research into thermal switches for reactor applications. It was subsequently employed by Marques [16] for a similar purpose, simulating the pressure and calandria tube of a CANDU reactor. The apparatus has three major sets of components: the experimental setup, the power control devices, and the data acquisition and management equipment. Two concentric horizontal cylinders immersed in a water barrel comprise the general configuration of the original experimental setup. At specific spots, both heater and pipe have thermocouples attached to their surfaces. A variable transformer (VARIAC) enables the operator to control power by changing the resistance to the voltage/current input. The electric circuit has two fuses in order to improve safety. The HP 3852A data acquisition unit allows the collection of data from

thermocouples and a digital pressure transducer. For the experiments described in the present report, the horizontal cylindrical tube was removed from the water barrel, and hung vertically from a frame, to simulate a vertical borehole. While the diameter of the apparatus is smaller than an actual borehole, the heater to outer cylinder gap is of the same thickness as found in the full scale application. Figures 3.1 and 3.2 show the overall layout of the apparatus, and more details can be found in [15] and [16].

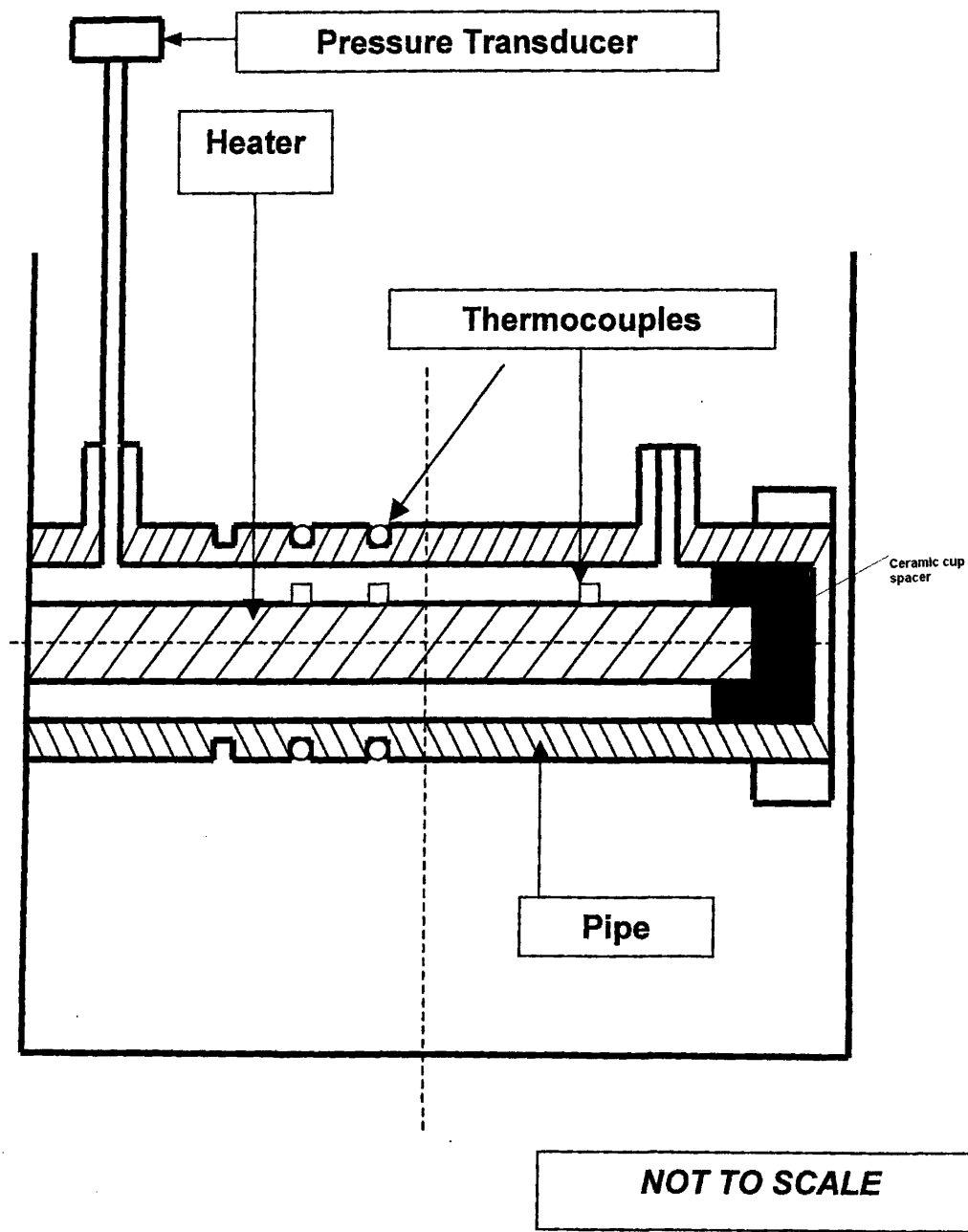


Fig 4.1 General Arrangement of Heater and Outer Pipe

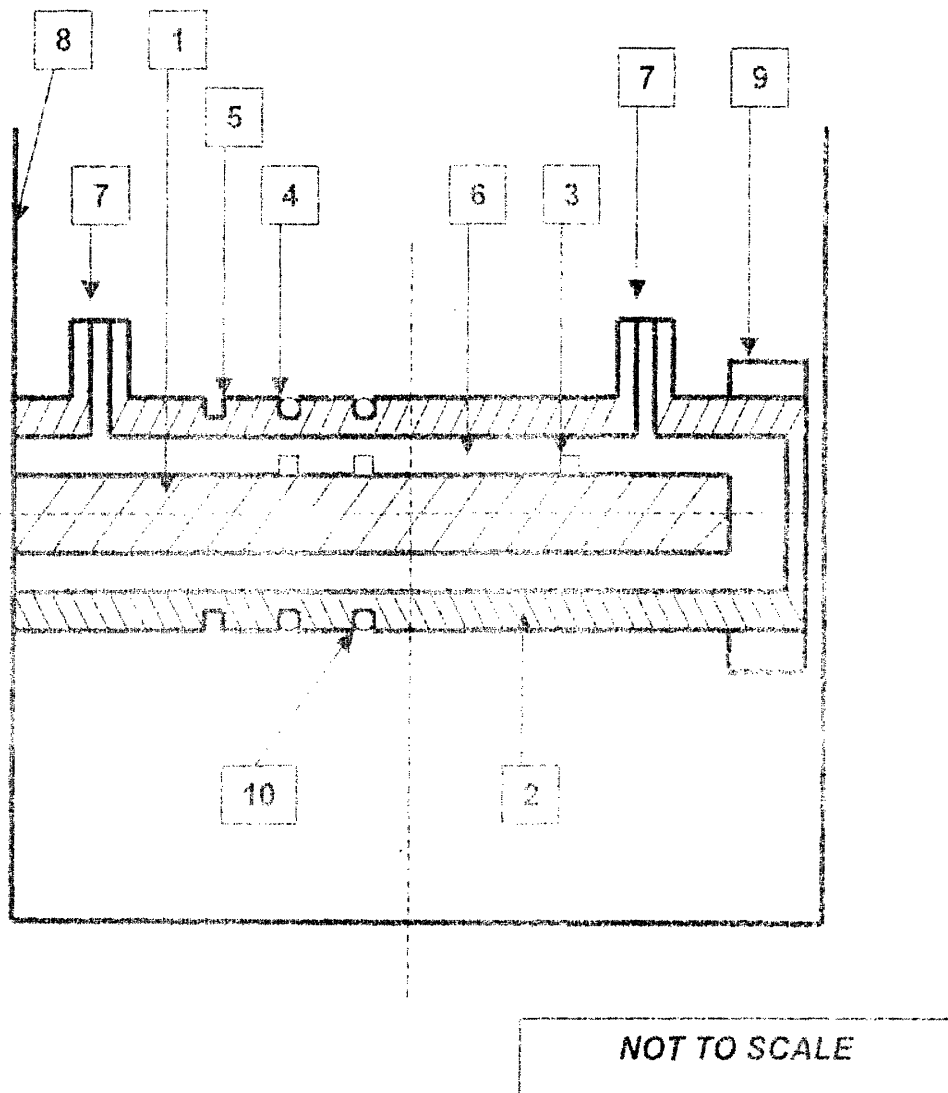


Fig 4.2 Specific Features of Heater and Pipe Configuration

(see text for discussion of labels)

The inner cylinder is an electrical heater that simulates the fuel rods and the pressure tube (label 1), and the outer cylinder is a pipe (label 2) that serves as an equivalent to the calandria tube in the original experiment. Both components are made of 304 stainless steel and have thermocouples at certain axial spots—six on the top of the heater surface (label 3) and eight on top of the external surface of the pipe (label 4). The thermocouples are attached inside circumferential grooves (label 5). The annulus between these cylinders (label 6) will be filled with various materials that will serve as the variables for our experiment which will be explained in greater detail later in this chapter. There are two hydraulic connections in the original setup (label 7). In the present experimental program however, we will not be employing them and thus they will be blocked. Label 8 and Label 9 show the water tank which serves as the heat sink, as well as one of the insulation devices, at one end of the experimental setup. The insulation prevents axial heat conduction. Finally, (label 10) shows a thermocouple positioned at the bottom of the pipe to measure the temperature at that region.

4.2.1 Configuration for Current Experiments

As noted earlier, for the present program, the heater and its annular surrounding cylinder were removed from the water barrel and hung vertically from an instrument rack. In addition the following items were modified or added.

- a) Air cooling system (a hinged 2 fan system) see Fig 4.3
- b) Suspension ropes attached to the top of support structure and to adjustable eyebolts see Fig 4.4

- c) Instrument rack used as support system; see picture in Fig 4.5
- d) New adjustable power supply (VARIAC) see Appendix B
- e) Power measurement meters: voltage and current see Fig 4.7
- f) Thermocouple readout see Fig 4.6

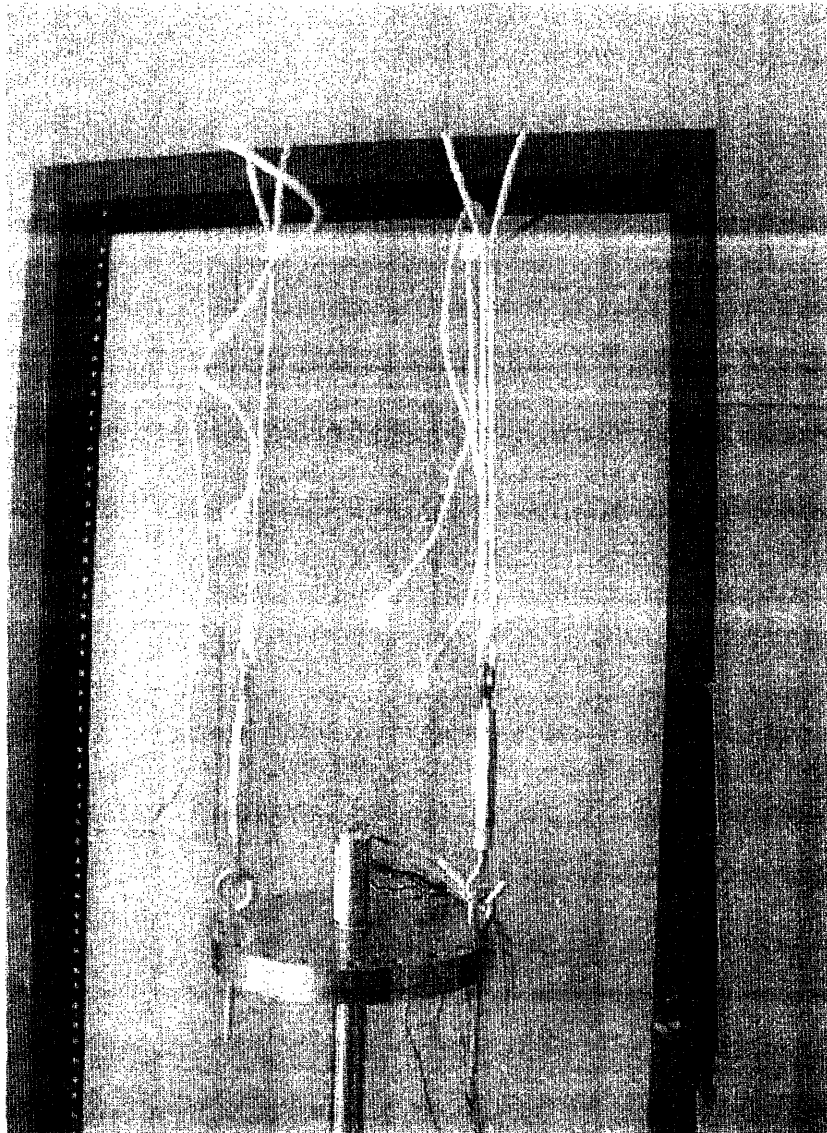


Fig 4.4 Picture showing Method of Vertical Suspension

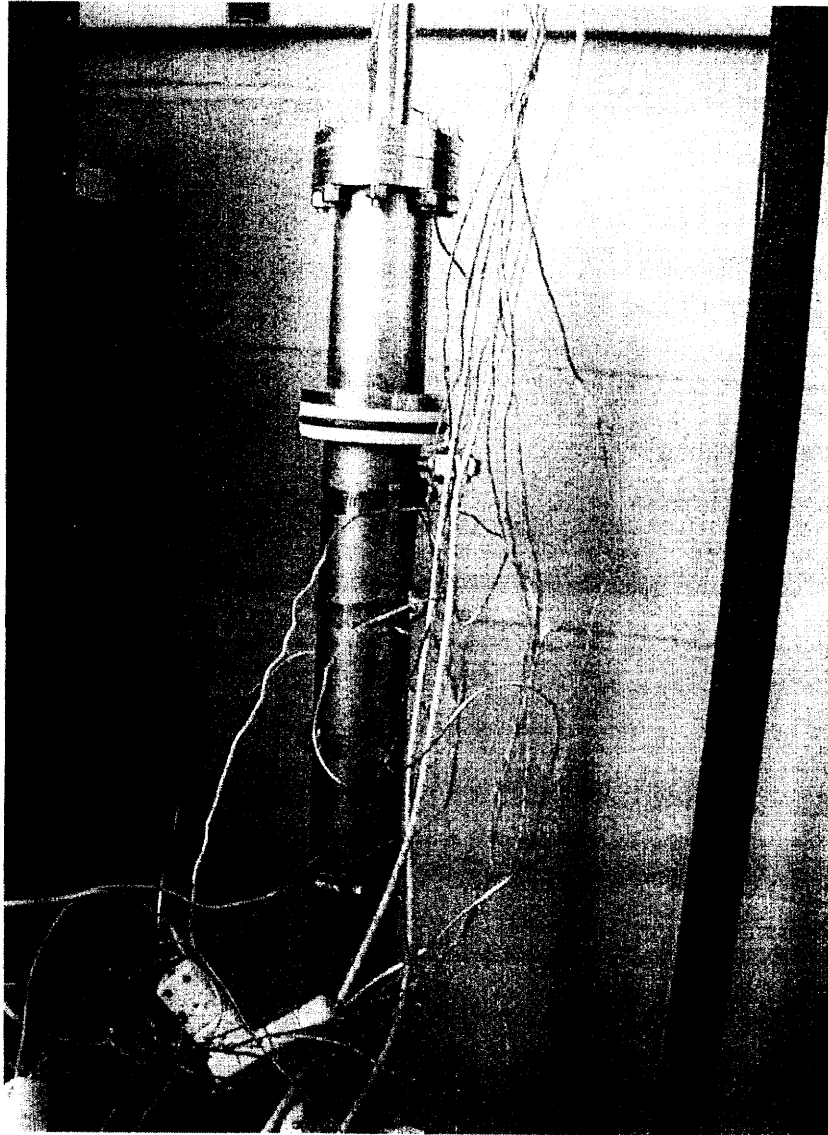


Fig 4.5 Picture of Heated Length of Apparatus

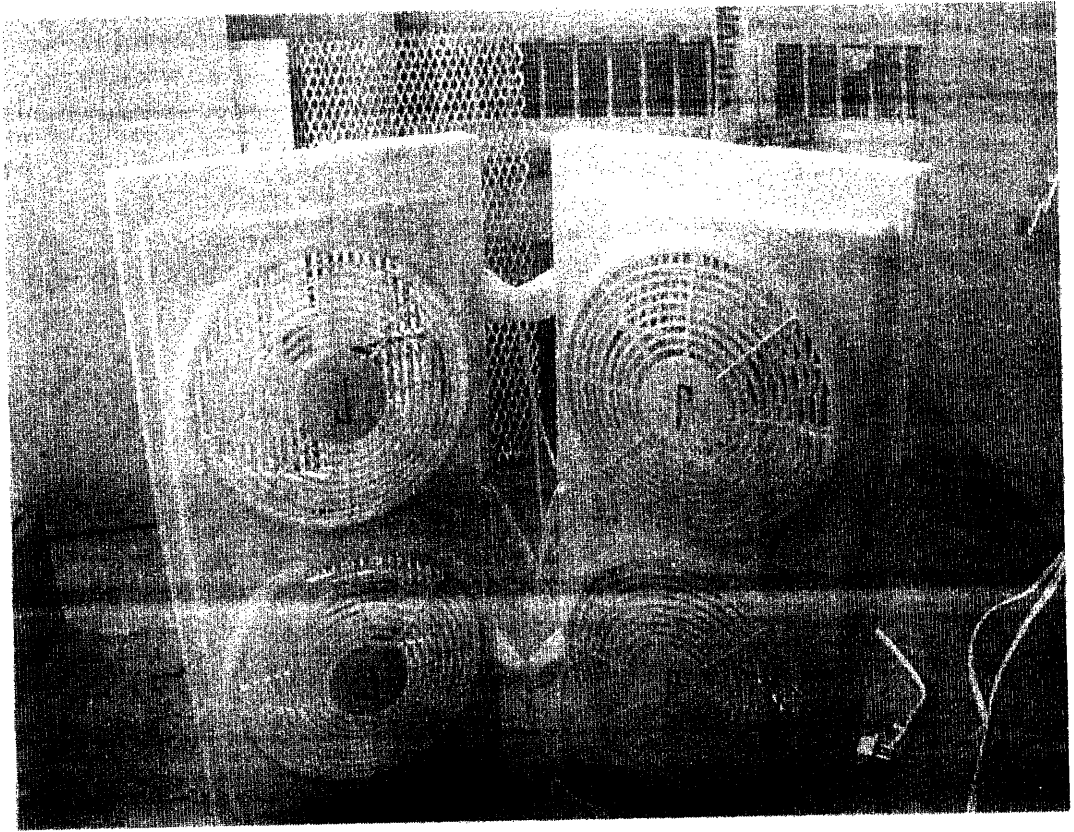


Fig 4.3 Fans Used to Cool Outer Cylinder of Heated Section

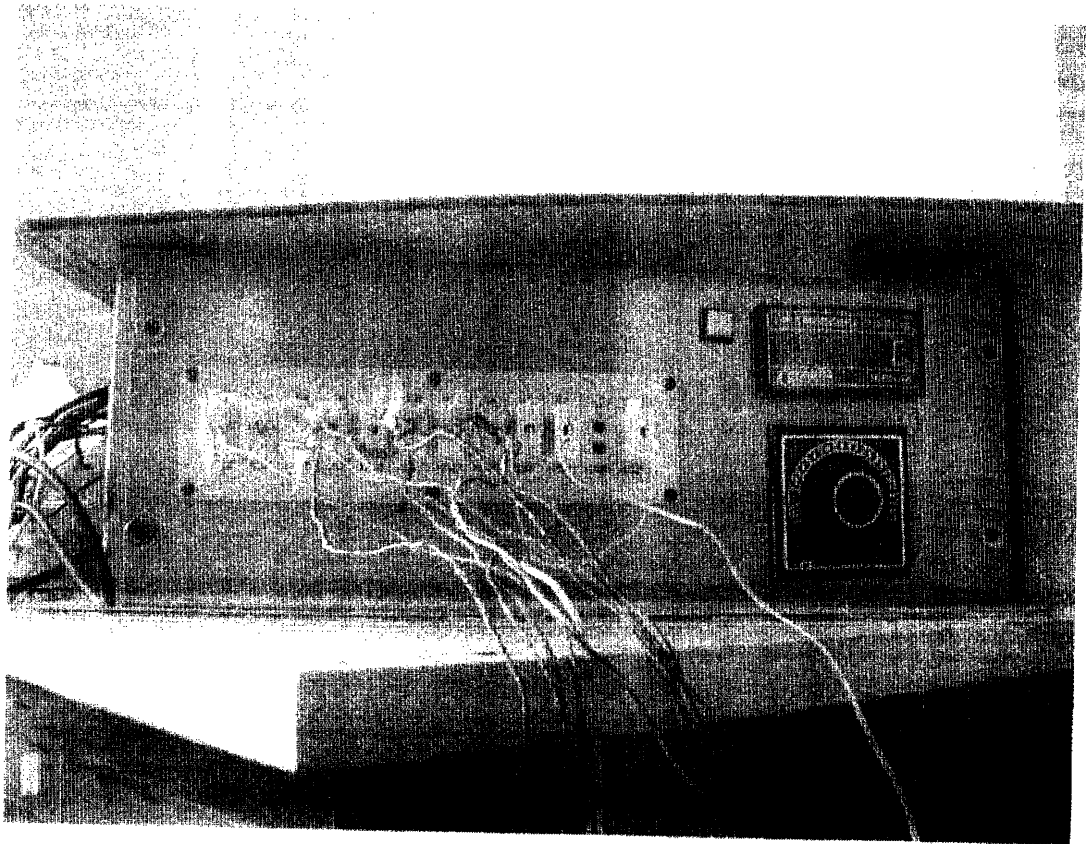


Fig 4.6 Picture of Thermocouple Readout

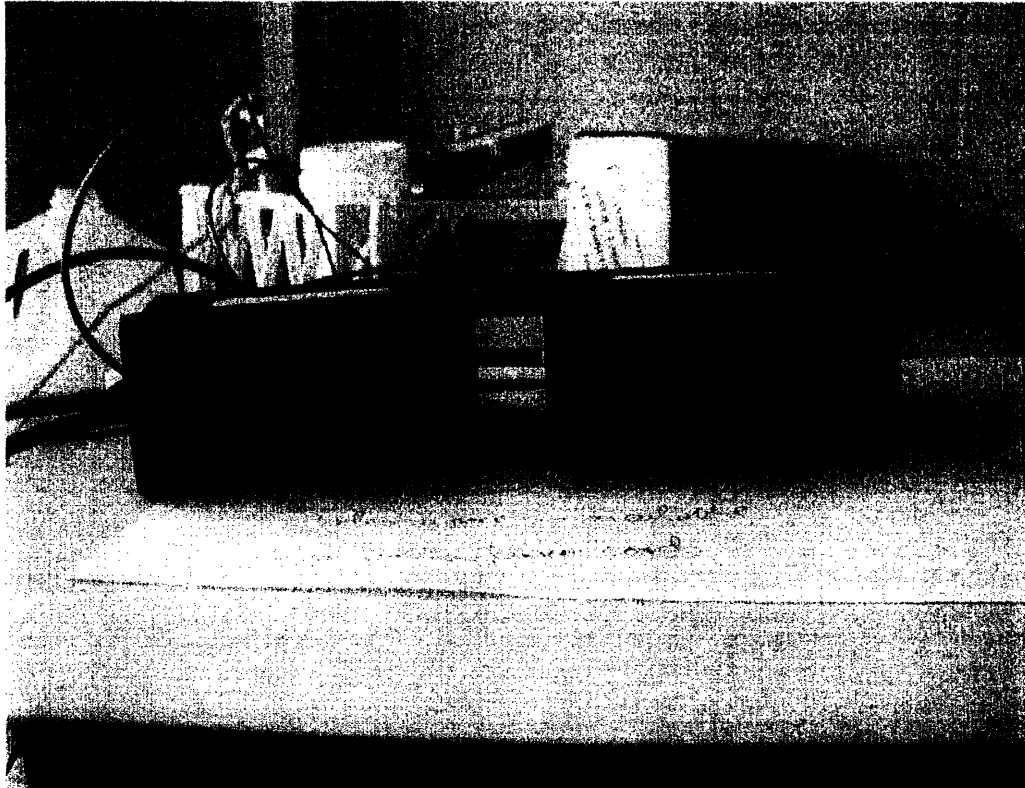


Fig 4.7 Picture of Ammeter and Voltmeter

Figure 4.8 shows the overall dimensions of the experimental setup. All logistical information about the hardware can be found in Appendix B. Table 4.1 shows the main numeric data.

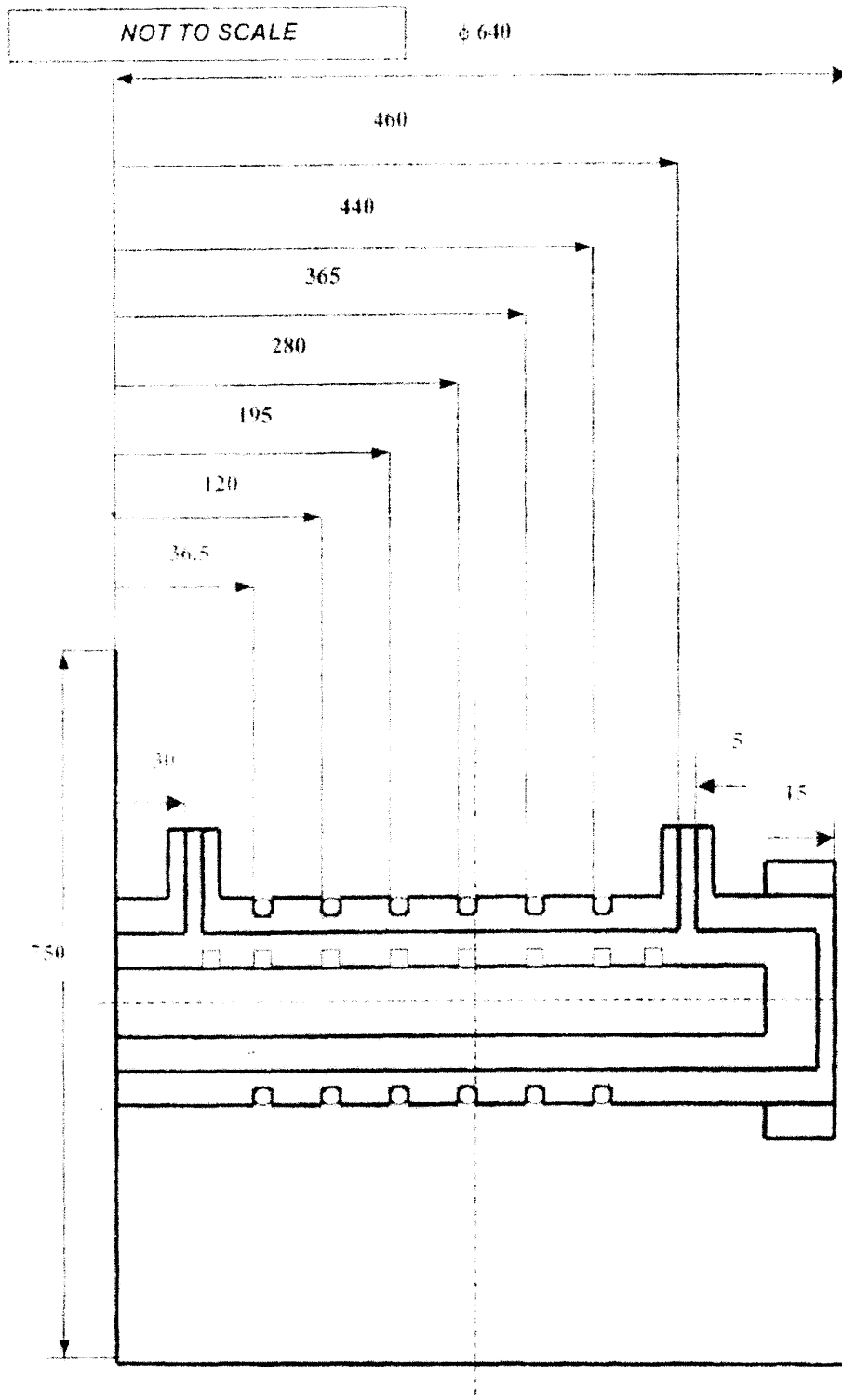


Fig 4.8 Experimental Setup: Overall Dimensions in mm

Table 4.1 Key Parameter for Test Rig

Characteristic	Units	Value
Maximum Electric Power	W	2200
Maximum heat flux @ the heater surface (calculated)	kW/m ²	83.80
Maximum current	Amps	5
Maximum voltage (lab wall power strip)	Volts	110
Heater length	m	0.457
Heater diameter	m	0.0254
Pipe inside diameter	m	0.052
Thickness of annulus gap	m	0.0133
Pipe thickness	m	3.175E-3

The maximum thermocouple temperature permitted is 500°C; in the present work this was limited to 300°C to preserve these instruments for extended use. Although the heater is rated to operate at 25 amps [16], the VARIAC maximum current is 20 Amps. With this configuration, the maximum electric power achieved has been limited to 2200W, corresponding to a maximum current of 19.5 Amps and a heater surface heat flux of 83.8 kW/m². However in practice, power levels greater than 98W were never required.

4.3 Testing Conditions

In order to define the experimental program, one should characterize deep borehole conditions, i.e heat fluxes, boundary conditions, and geological environment, that can be represented by the experimental setup above at a smaller scale. Deep borehole far-field temperatures are about 100°C- 300°C, due to the geothermal gradient of about 25°C/km. As will be seen, the heater in the experiment will usually experience a maximum surface temperature of 100°C, suitable since material properties do not change much over 100°C- 200°C. Considering characteristics of the conceptualized deep boreholes described in the literature reviewed in Chapter 2 the values in Table 4.2 are representative:

Table 4.2 Typical deep borehole and experimental setup data

Characteristics	Actual deep borehole	Experimental setup
Diameter of Borehole	214mm	52mm
Height of Canister and fuel assembly	5m	0.457m
Max centerline temperature (Typical)	337°C	100°C (heater surface)
Max borehole wall temperature (Typical)	240°C	55°C
Heat flux W/m ² , max	446	83.80
Linear Power W/m, max	300	125
Gap: heater or canister to wall	0.033m	0.0133m
Ambient Pressure	100MPa (max)	0.1 MPa

Since axial thermal conductivity is not significant in either an actual canister or our heater, attention will be concentrated on radial conduction. The experiment will simulate thermal conductivity through approximately one centimeter of material, which is on the same order as would be encountered in a borehole. Material properties do not vary significantly over the range of temperatures shown. Hence the experiment is an acceptable physical analogy. Finally, the most important parameters: gap thickness and surface heat flux are sufficiently similar.

The experimental setup does not take into account that in an actual deep borehole system underground pressure reaches lithostatic levels. However these pressures only affect convection heat transfer modes that deal with gases. In our system liquids and solids are the predominant states we will be dealing with. With solids, the dominant mode of heat transfer is conduction, where lithostatic pressure has little or no effect, nor does pressure convection in liquids. For gases thermal conductivity is approximately proportional to absolute temperature to the $3/2$ power, and independent of pressure. Hence the proposed measurements are considered conservative, and will in fact be characteristic of times immediately following emplacement. Because we will be making thermal conductivity measurements, the measurements will be taken when the system reaches steady state.

The experimental program will focus on measuring parameters needed to evaluate thermal aspects of the deep disposal of nuclear spent fuel in particular geographical environments: specifically, different materials that may be used as fill in deep boreholes or in-canister packing. These materials are silicon carbide, aluminum, graphite and others. We will also be making several assumptions in doing the experiment. For

example, it is assumed that the nuclear spent fuel will have 10 years of cooling time before the spent fuel will be buried. For maximum burnup of 60,000 MWd/kg, this leads to canister linear power of 300 W/m and heat flux of 446 W/m² for a 0.214m diameter canister. [16].

4.4 The Experimental Program

4.4.1 Introduction

Due to the complexity of the heat transfer phenomena involved, the only reliable way to quantify the system heat transfer behavior is by testing under conditions that can be extrapolated to the real conditions. Modeling and manipulation of theoretical equations is not enough to consider all the details involved, such as particle contact resistance or particle to wall thermal resistance, surface emissivities when radiation is important, and convection in annular gaps.

Thus the experimental program has its main objective and the measurement of the effective overall thermal conductivity for several materials of interest in an annulus under boundary conditions as close as possible to the actual deep disposal waste scenario. The values so obtained can be used to assess the performance attributes of the deep borehole waste disposal concept with a much greater assurance of reliability.

4.4.2 The Variables

The main variable in this experiment is the nature of the material in the gap, in the present work this will include materials such as: granular silicon carbide, other particle beds, air and water.

In this experimental work, the overall heat transfer coefficient (h) has the following definition in W/m^2K :

$$h = P / [A_{\text{heater}} * (T_{\text{heater}} - T_{\text{heat sink}})] \quad \text{eqn. 4.1}$$

Where

P – electric power (W)

A_{heater} - heater surface area (m^2)

T_{heater} – heater surface temperature (K)

$T_{\text{heat sink}}$ – outer tube of apparatus temperature (K)

In order to determine h , the level of material filled between the annulus will remain the same for each material tested and exceed the active length of the heater. The electric power use will vary, three different voltage percentages¹ (Variac settings) will be used: approximately 5%, 10%, and 20%. Each of these settings will be use for each material being tested. Figure 3.5 shows a schematic with the thermocouple locations indicated. It represents a cross-section of the experimental setup, under the hypothesis that there is no significant axial temperature variation. See appendix A. for plots showing axial temperature variation.

The variables to be measured are:

- a) Heater thermocouple temperatures

¹ On scale of 0-100 % reading corresponds to roughly 1 volt per 100%.

- b) Pipe thermocouple temperatures
- c) Variac Setting (%)
- d) Current of electric power (Amps)
- e) Voltage of electric power (Volts)

The experimental routine can be summarized as:

- a) Fill annular gap with material to be tested and seal
- b) Set the initial run conditions:
- c) set approximate specified electric power level by turning the VARIAC dial; record actual power as indicated by the product of voltmeter and ammeter readings.
- d) Log data when temperatures of each thermocouple have reached steady-state; the steady-state condition is assumed when there is, at maximum, a temperature variation of plus $\pm 2^{\circ}\text{C}/\text{hour}$. When this condition is reached, recorded data over a 15 minute period.
- e) The thermocouple temperatures are to be listed in pairs corresponding to those straddling the gap at the same positions namely: 2 and 12; 11 and 3; 10 and 4; 9 and 5.
- f) Repeat for three power levels: VARIAC settings of 20 V, 10 V., and 5 V., which translates to approximate power levels of 94W, 24W and 7 W respectively

4.5 Data

A typical raw data set will look like figure 4.9. These raw data tables are collected in Appendix C. The processed data is presented subsequently in this chapter.

Date		7/19/2006
Trial #		1
Time		2:00pm
Material		aluminum
Variac		10%

Experimental Data	
Run #	1
ACA	1.7
ACV	15.2
Power, W	25.84
Thermocouple #	Degrees in Celsius (°)
1	42
2	47
3	50
4	52
5	51
6	47
7	45
8	42
9	33
10	34
11	35
12	35

Analysis	
Average Tube T	34.25
Average Heater T	50
ΔT (average)	15.75
Heat flux	689.0667
h	43.75026

Fig 4.9 Typical Raw Data Set for a Run

The column labeled “thermocouple #” lists the numbers that correspond to the thermocouple designations located in Figure 4.5.2. Since there are limited outer thermocouples (those attached to the outer tube of the apparatus), analysis will be limited to those thermocouples which have corresponding inner thermocouples located in the heater.

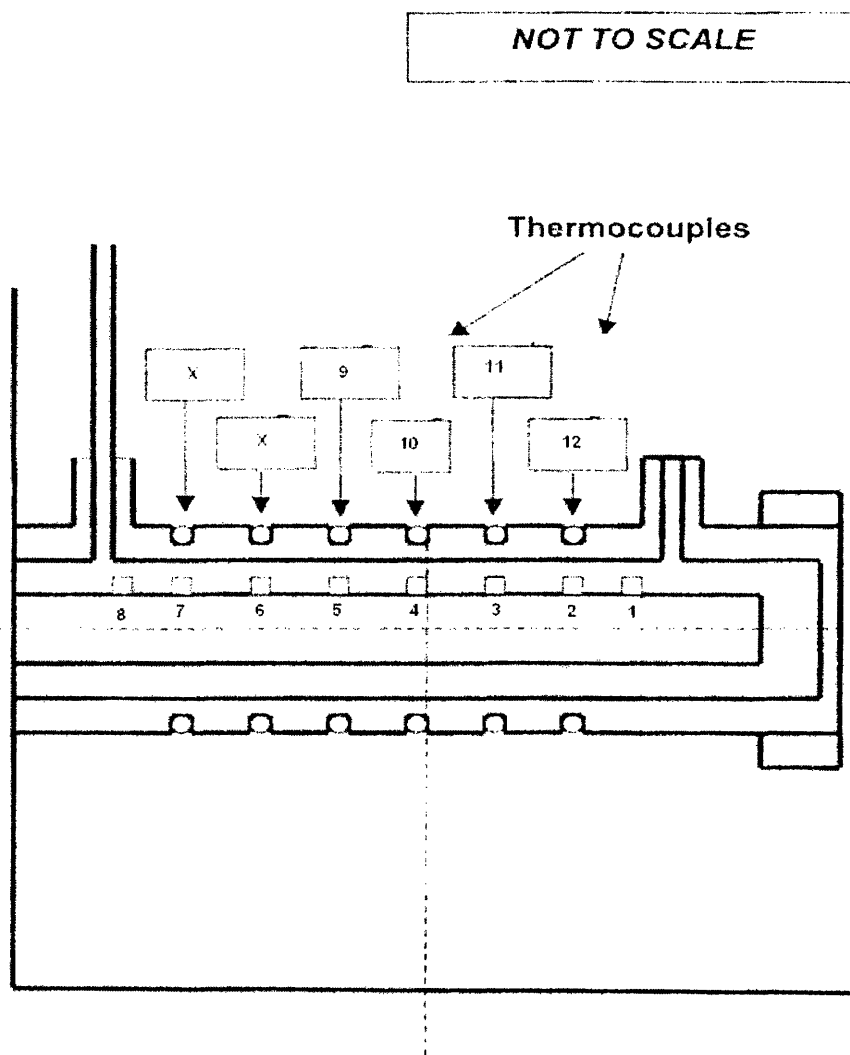


Fig 4.10 Specific Thermocouple Locations Used for Data Analysis

Looking at Figure 4.5.1 and 4.5.2 the following are designated as outer thermocouple and inner thermocouples.

Inner thermocouples: #1-#8

Outer thermocouples:#9-#12

Pairing of thermocouples is as follows:

2 and 12; 11 and 3; 10 and 4; 9 and 5

Analysis

In analyzing the data, the four outer thermocouples (and inner thermocouples) are averaged and the difference between the average is recorded as a temperature difference.

Note that, mathematically, the difference of the averages is exactly the same as the average of the differences.

The heat transfer coefficient is computed from the measured data as follows where (see table 3.1)

$$h = P / [A_{\text{heater}} * \Delta T], \text{ W/m}^2 \text{ } ^\circ\text{K} \quad \text{eqn. 4-2}$$

l (heater length): 0.47m

d (heater diameter): 0.0254m

A (heater area): 0.0365 m²

P, power: ACA(value)*ACV(value)

ΔT = difference between the averages of inner and outer thermocouple readings, ° K

Heat flux: power/0.0375m²

h: heat flux/ ΔT (average)

Alternatively one can calculate the effective thermal conductivity as follows:

conduction between the heater inner and outer surface of an annulus satisfies the relation:

$$k = \frac{P * \ln(re / ri)}{2 * L * \pi * \Delta T} \quad \text{eqn. 4-3}$$

Where

P - thermal power, W

re - inner radius of the cylinder wall (m);

ri – outer radius of the heater (m);

L – cylinder length (m);

k – thermal conductivity of the test material (W/m. K)

ΔT – temperature difference between the heater temperature and inside surface of the cylinder wall.

Thus $k = \frac{h * di * \ln(de / di)}{2} = h * ri * \ln(re / ri) = 0.0091 * h$ eqn. 4-4

Thus k is a constant times h

4.5.1 Overall Heat Transfer Coefficient

Tables 4.5.1a to 4.5.1e show the values of h and k for the different power levels and materials tested. Test identification is noted with materials inside, power level, steady state thermal conductivity and heat transfer coefficient (Appendix B describes the material in some detail). Appendix C tabulates the raw data and also analyzes the uncertainties of the measurements. For each data set the results are plotted and show linear dependence versus temperature differences within experimental uncertainty. This shows that changes in the phenomena or properties with temperature and temperature difference is small, and that assuming constant h and k are adequate for our purpose.

Defined values used in the tables and graphs which follows are:

$$Q \text{ (W/m)} = P \text{ (power shown in Fig 4.5)} / \ln(r_e/r_i) / 2 * L * \pi$$

$$\ln(r_e/r_i) / 2 * L * \pi = 0.25$$

$$\Delta T \text{ (}^\circ\text{K)} = \text{from Fig 4.5}$$

$$Q \text{ (W/m)} / \Delta T \text{ (}^\circ\text{K)} = k \quad \text{eqn 4-5}$$

$$\text{Conductivity (k)} = 0.0091 * h \text{ (from eqn 4-4)}$$

Fig 4.5.1a Q vs. Delta T: Effective k for Air

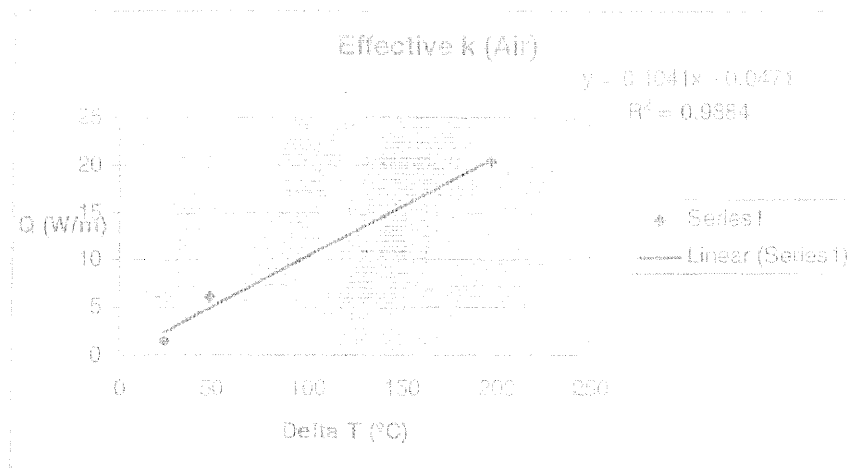


Table 4.5.1a k and h versus power for Air

Power (W)	Conductivity (k), W/mK	h (W/m ² K)
5.75	0.056	6.39
29.49	0.070	8.00
77.65	0.092	10.48
Average	0.073	8.29
Slope from graph	0.104	10.5

Table 4.5.1b k and h versus power for Silicon Carbide Sand

Power (W)	Conductivity (k), W/mK	h (W/m ² K)
7.36	0.314	35.68
26.66	0.278	31.6
89.78	0.323	36.69
Average	0.305	34.66
Slope from graph	0.366	37

Fig 4.5.1b Q vs. Delta T; Effective k for SiC

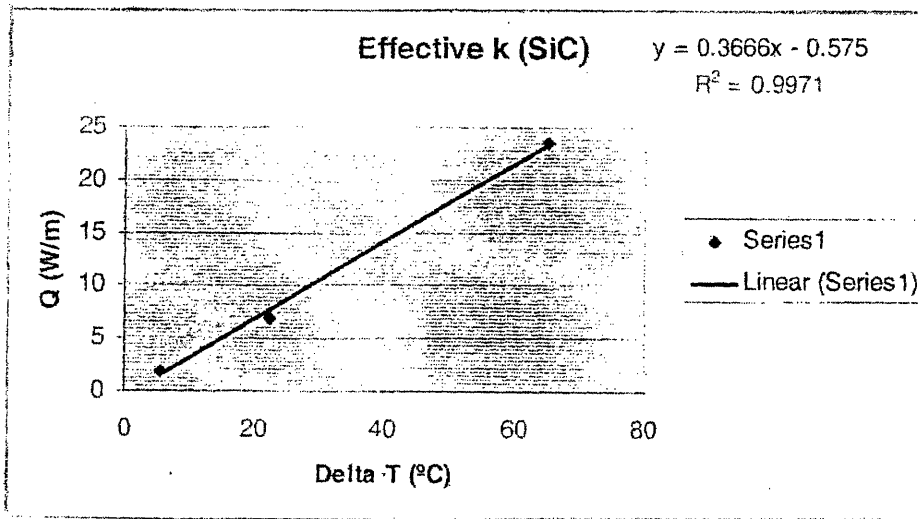


Table 4.5.1c k and h versus power for graphite sand

Power (W)	Conductivity (k), W/mK	h (W/m ² K)
7.2	0.338	38.4
25.67	0.376	42.78
96.14	0.396	45.00
Average	0.370	42.06
Slope from graph	0.449	45.4

Fig 4.5.1c Q vs. Delta T; Effective k for Graphite sand

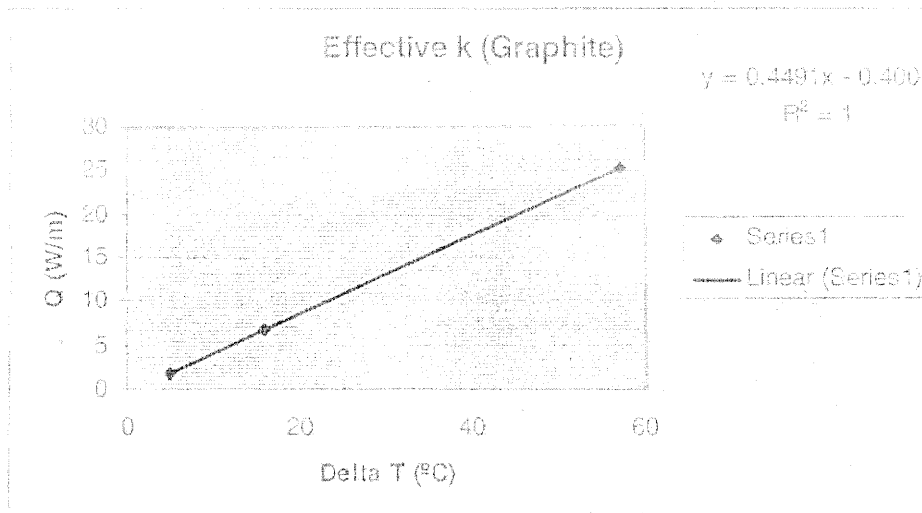


Table 4.5.1d k and h versus power for Aluminum powder

Power (W)	Conductivity (k), W/mK	h (W/m ² K)
7.54	0.506	57.5
25.84	0.385	43.75
98.01	0.541	61.5
Average	0.477	54.25
Slope from graph	0.624	63

Fig 4.5.1d Q vs. Delta T; Effective k for Aluminum Powder

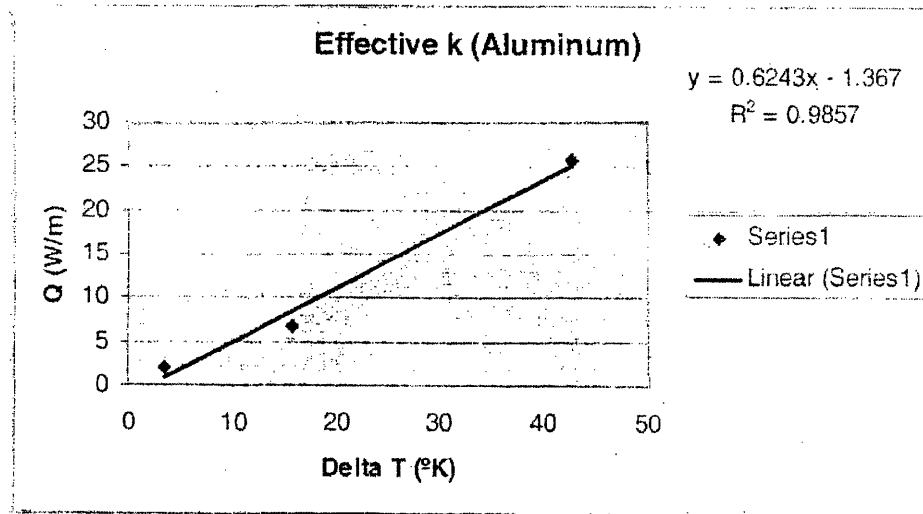


Table 4.5.1e k and h versus power for Metal Sleeve

Power (W)	Conductivity (k), W/mK	h (W/m ² K)
9.08	0.059	6.72
23.80	0.064	7.38
95.26	0.091	10.41
Average	0.071	8.17
Slope from graph	0.111	11.21

Fig 4.5.1e Q vs. Delta T; Effective k for Metal Sleeve

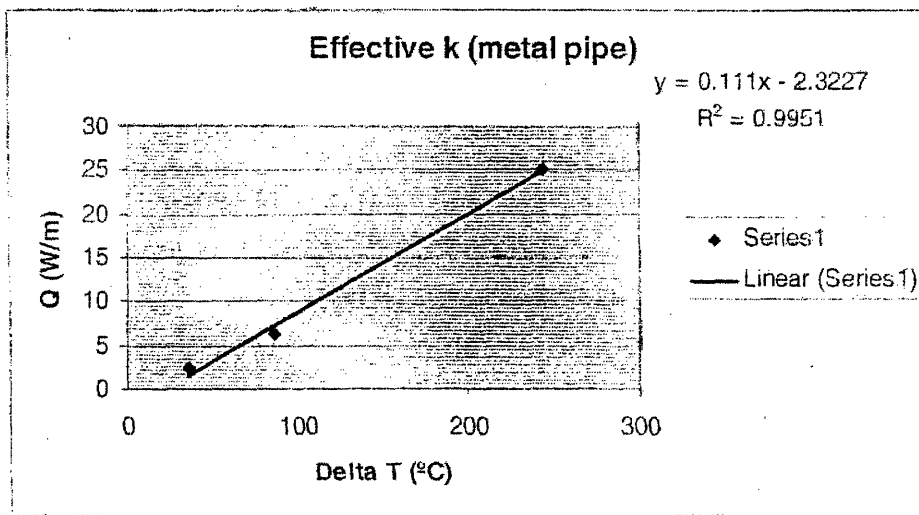


Table 4.5.1f k and h versus power for Water as material in annulus

Power (W)	Conductivity (k), W/mK	h (W/m ² K)
6.86	2.15	244.05
23.80	2.23	253.85
90.95	3.28	373.12
Average	2.55	290.34
Slope from graph	3.93	397

Fig 4.5.1e Q vs. Delta T; Effective k for Water

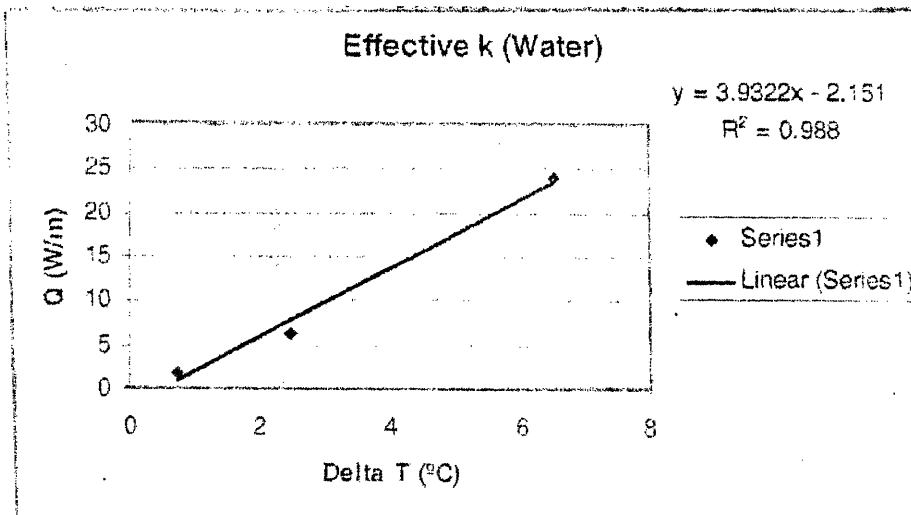


Table 4.5.1g k and h versus power for Sand

Power (W)	Conductivity (k), W/mK	h (W/m ² K)
6.22	0.364	41.44
24.73	0.347	39.38
96.76	0.398	45.27
Average	0.369	42.03
Slope from graph	0.455	46

Fig 4.5.1e Q vs. Delta T; Effective k for Sand

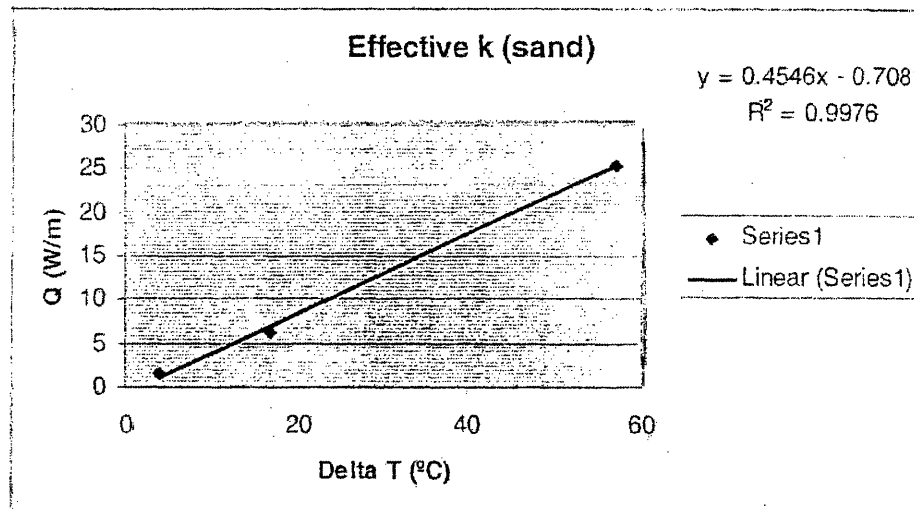


Table 4.5.1h show the average values for h and k of different fill materials within the annulus of the experimental set up. Their significance will be discussed in Chapter 5.

Table 4.5.1h : average h and k as a function of material tested in annulus

Material	h (W/m ² K)	k (conductivity), W/mK
Air	8.3	0.073
Silicon carbide	35	0.31
Graphite	42	0.37
Aluminum	54	0.48
Water	290	2.55
Sand	42	0.37
Metal Sleeve	8.2	0.07

4.6 Chapter Summary

This chapter presented the experimental setup and the experimental program and its results in evaluating suitable material for removal of decay heat in order to prevent damage to the waste form. The main heat transfer parameters were identified as the overall heat transfer coefficient (h) and thermal conductivity (k), between the heat source (heater) and heat sink (annular tube in the present instance). The results were presented in the form of tables of h and k versus power (for specific materials), h and k versus material (for specific power levels) and the best estimate (average) values of the

parameters. Graphs also presented the effective thermal conductivity (k) for each material tested, as the (close-to) linear slope of power vs. ΔT plots.

- a) **Convection**- This mode is always seen when fluid motion occurs. In the experimental setup, convection can occur in the medium (e.g. air or water) between the heater and the annulus inner wall, and between the external surface of the pipe and the ultimate heat sink (ambient air).

The general equation that represents convection follow Newton's law of cooling and can be stated as

$$q_s = h_c * (T_{\text{heater}} - T_{\text{heat sink}}) \quad \text{eqn. 5-3}$$

Where

- a) Q_s = ratio between thermal power (W) and it's surface area (m^2)
 - b) h_c * is defined as the heat transfer coefficient ($W/m^2 K$), which is normally given by correlations of experimental data
 - c) T_{heater} – heater surface temperature (K)
 - d) $T_{\text{heat sink}}$ – outer tube of apparatus (inner surface) temperature (K)
- b) **Conduction** –This mode is observed when heat is transferred through a fluid or solid. In the experimental setup, the pipe is made of stainless steel, which has a high thermal conductivity. Also, test material within the annulus is subjected mainly to thermal conductivity. Therefore, the difference in temperature between the inner surface and the outer surface of the pipe should be small for the pipe and can be neglected, in which case the equation that represents the heat transfer through the annulus to the pipe is as previously given in Eqn. 4-1.

$$k = \frac{(Q/L) * \ln (R_2/R_1)}{(2\pi \Delta T)} \quad \text{eqn. 5-4}$$

Where

Q - thermal power

R_2 – inner radius of the cylinder wall (m);

R_1 – outer radius of the heater (m);

L – cylinder length (m);

k – thermal conductivity of the test material (W/m. K)

ΔT – temperature difference between the heater surface and inner surface of the cylinder wall.

- c) **Radiation** – This heat transfer mode occurs by propagation of electromagnetic waves (radiation) between two bodies that are at different temperatures, and separated by a transparent medium. The energy flux leaving a surface due to emission and reflection of electromagnetic radiation is named “radiosity” (W/m^2). The Stefan-Boltzmann law applies and the thermal power transmitted by radiation is proportional to $(T_{\text{heater}}^4 - T_{\text{heat sink}}^4)$. Due to the low difference of temperatures between the heater and the heat sink observed in the experiments, radiation heat transfer is small (but still significant) see Appendix A and section 3.2.2. Furthermore, only in the air-filled annular gap is it present: water or particle beds effectively eliminate this mode of heat transfer.

Only convection and conduction will be considered in the analysis of h. Using concepts and equations presented above, the heat transfer modes have the following components:

- a) Convection between the heater and the material (for this experiment it will be restricted to mainly air and water) inside the annulus:

$$P = h_h [A_{\text{heater}} * (T_{\text{heater}} - T_{\text{heat sink}})] \quad \text{eqn. 5-5}$$

Where

h_h – heat transfer coefficient between the heater and the material inside the annulus;

P – electric power (W);

A_{heater} - heater surface area (m^2);

T_{heater} – heater surface temperature (K);

$T_{\text{heat sink}}$ – outer tube of apparatus (inner surface) temperature (K);

b) Conduction between the heater and the material (for this experiment it will be restricted to mainly solid particles i.e, silicon carbide, graphite, sand and aluminum), (where thermal contact resistance between the metal surfaces and the bed of particles is included).

$$P = \frac{\Delta T}{\frac{\ln(re / ri)}{2 * L * \pi * k}} \quad \text{eqn. 5-6}$$

Where

P - thermal power

re - inner radius of the cylinder wall (m);

r_i – outer radius of the heater (m);

L – cylinder length (m);

k – thermal conductivity of the test material (W/m. K)

ΔT – temperature difference between the heater surface and inner surface of the cylinder wall.

5.3 Overall Thermal Conductivity as a Function of Material Tested

Table 5.3.1 is a Table of thermal conductivity as a function of material tested.

The average values are cited (see chapter 4)

Table 5.3.1 materials tested and their effective thermal conductivity

Material	Conductivity (k) W/mK
Air	0.073
SiC	0.31
Graphite	0.37
Aluminum	0.48
Water	2.55
Sand	0.37
Metal sleeve	0.07

Water has the highest thermal conductivity of the materials due to the added effective conductivity of convection, and aluminum powder has the highest conductivities of the solid particle beds. In chapter three, analytical estimates were made for some of these particles. Our silicon Carbide measurement yielded an effective thermal conductivity of 0.31 and the analytical estimate in table 5.3.2 was 0.33. This should be considered as within the uncertainty of both the analytical estimate and the measurement. Sand and graphite are comparable.

What Results Mean for Deep Borehole Concept

Given our experimental findings for thermal conductivities, we can explain what the measurements imply for the deep borehole concept. They are listed below:

- 1) Any and all particle beds are better than air-only, even sand. Most beds have roughly the same k.
- 2) Graphite is a good candidate for filling gaps, to increase k, hence reduce ΔT , by a factor of more than 5. It should also act as a lubricant to make retrieval easier.
- 3) We don't have to worry about sand or gravel falling into the canister/borehole gap from a thermal point of view; but it would hinder retrievability.
- 4) Flooding with water would be very beneficial from a thermal point of view; a factor of 35 reduction in ΔT within the gap. The principal concern would be its effect on corrosion, solubility and transport of waste radionuclides.

5) Nested cylinders separated by gas-filled gaps increase gap ΔT very little.

This should be contrasted to the large effect in a vacuum, which is exploited in Dewar design.

6) SiC would appear to be suitable to fill the void space between fuel pins inside a canister as a measure to increase crush resistance, but sand might do as well, and would be much cheaper.

5.4 Chapter Summary

In general, the results confirm the estimates used by Hoag [4] (and earlier by Kuo [14]), in overall canister and borehole design, hence validate their estimates of satisfactory performance.

Chapter 6

Summary, Conclusions and Recommended Future Work

6.1 Summary and Conclusions

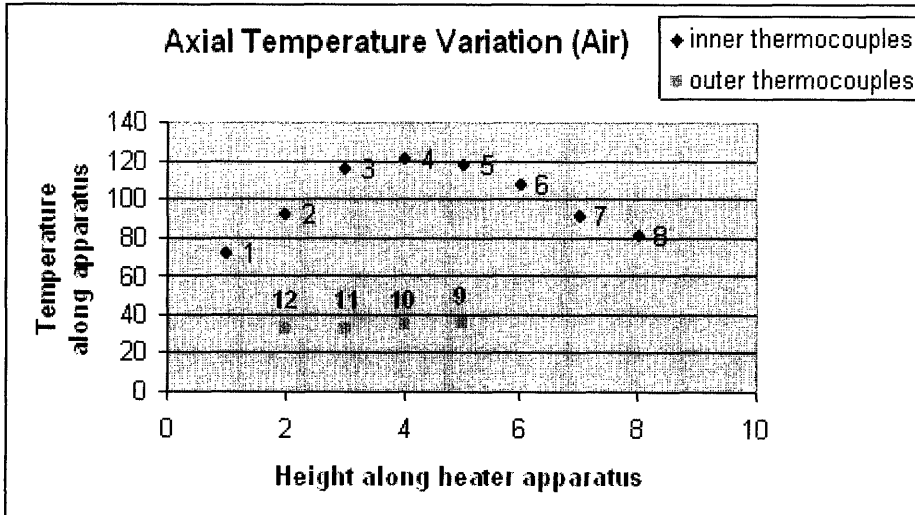
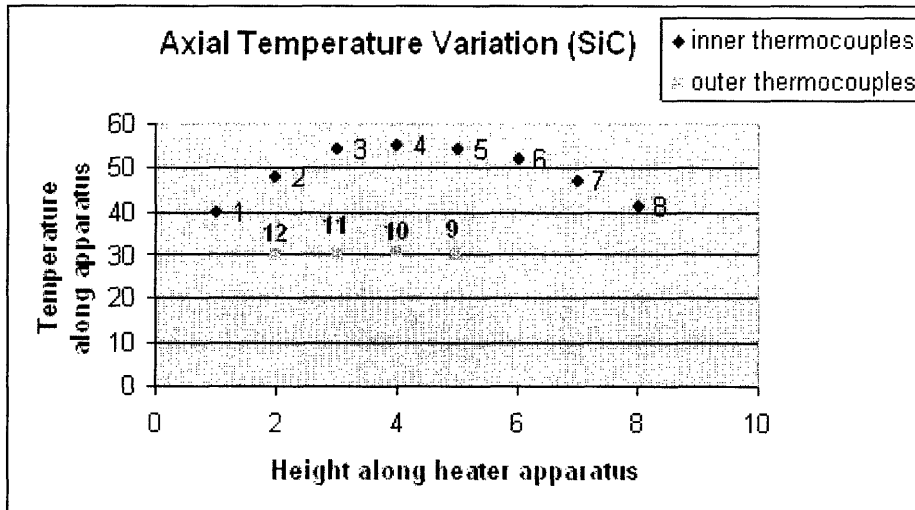
The main focus of this thesis was to determine experimentally, overall heat transfer coefficients under different operational conditions. The heat transfer results in general are on the same order as the literature values as shown in table 5.3.2.

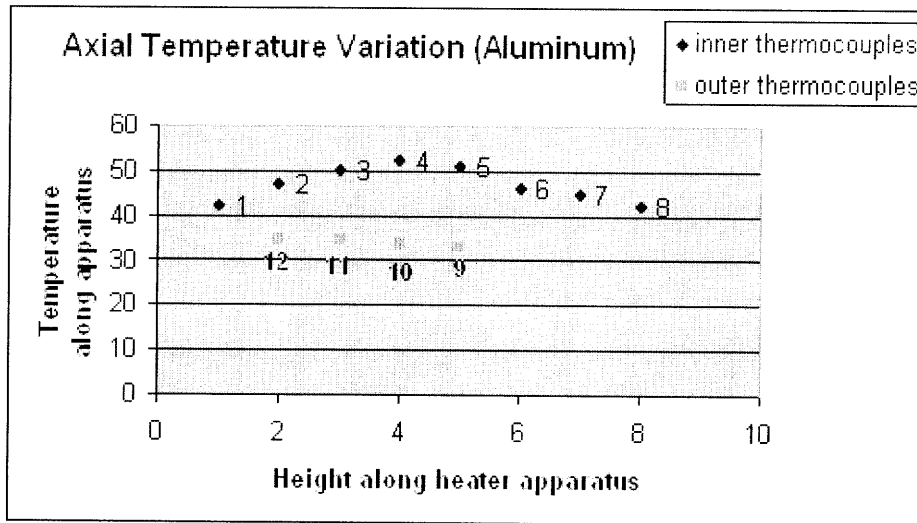
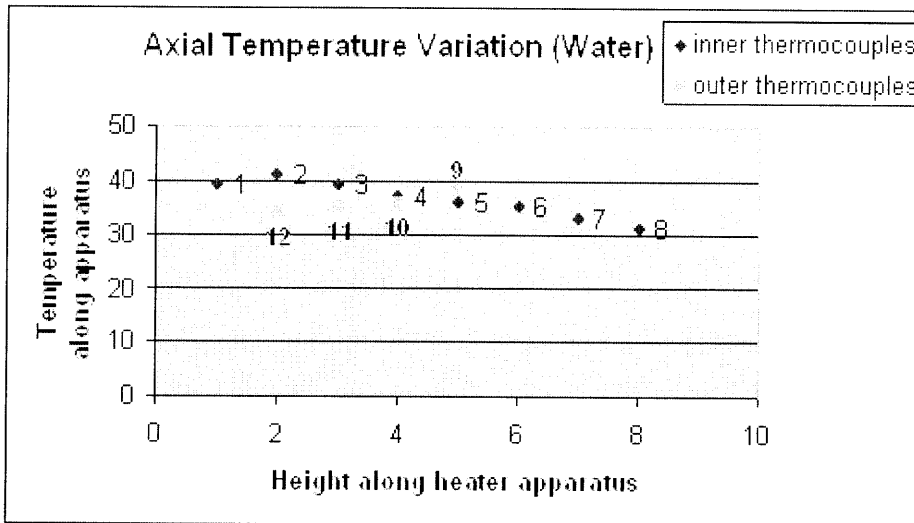
6.2 Future Work

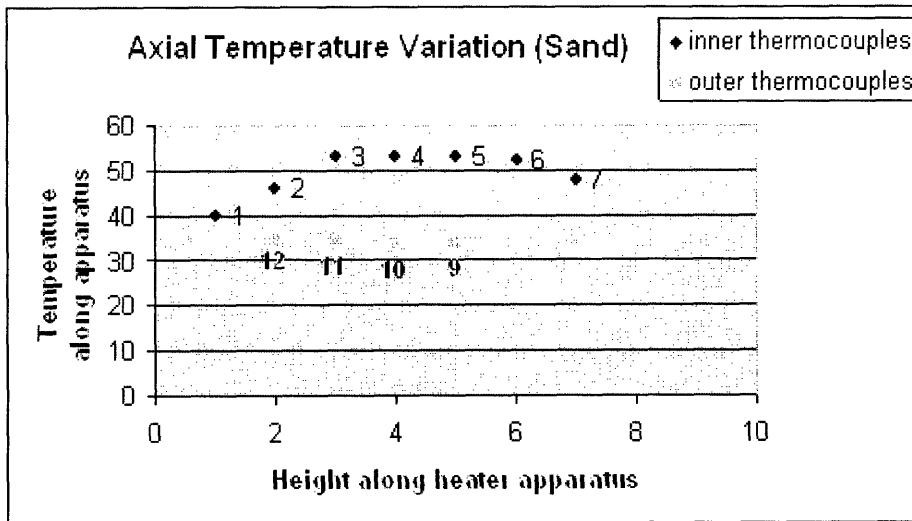
There were a couple of aspects that were not investigated that could be addressed in a follow-on project. First, repeat experiments were not conducted that could be done in future experiments to check on reproducibility; also different materials could be used within the annulus, for example, cement or grout. This will require re-design of the outer pipe so that it can be easily removed (eg. cut in half longitudinally). Other test material options would be to use different fill gases, such as helium. For example, sand plus helium appears to be good candidate for filling the void space inside a canister's fuel bundle.

Appendix A: Calculations

A.1 Plots showing axial temperature variation for different materials







Looking at the graphs above, inner thermocouples 1 and 2 show significant axial temperature differences. In the future the thermocouple pair 2 and 12 should be dropped in the calculations of ΔT . In our results this axial temperature difference will increase our inferred conductivity slightly.

A.2 Void space calculations of experimental particle beds

In order to calculate void space we used a 100ml glass cylinder and recorded its weight, then filled the cylinder with the particle bed to the “100ml” mark and recorded its weight. The next step is to add water slowly to the particle bed sample until it is saturated with water, and record its weight. The weight of the water gives the void space of the particle bed.

Void space of Graphite

100ml glass cylinder: 102.2g

100ml glass cylinder + graphite powder= 181.2g

100ml glass cylinder + graphite powder + Water used= 224.7g

Water used= void space= 43.5g =43.5cc

Void space fraction= water used/ 100cc=43.5%

Void space of Aluminum

100ml glass cylinder: 102.2g

100ml glass cylinder + Aluminum powder= 235.8g

100ml glass cylinder + Aluminum powder + Water used= 286.4g

Water used= void space= 50.6g= 50.6cc

Void space fraction= water used/ 100cc=50.6%

Void space of Sand

100ml glass cylinder: 102.2g

100ml glass cylinder + Sand= 274.2g

100ml glass cylinder + Sand+ Water used= 313.7g

Water used= void space= 39.5g= 39.5cc

Void space fraction= water used/ 100cc=39.5%

Void space of Silicon Carbide

100ml glass cylinder: 102.2g

100ml glass cylinder + Sand= 274.2g

100ml glass cylinder + Sand+ Water used= 315.4g

Water used= void space= 40.6g= 40.6cc

Void space fraction= water used/ 100cc=40.6%

Appendix B Description of Materials and Apparatus

B.1 Test Material Description

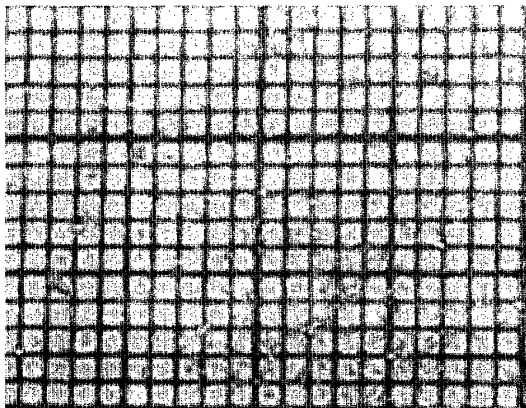


Figure above is an image of Aluminum powder spread on a 1 mm. sq. grid

Material: Aluminum powder, Irregular shape, rhombic broken crystals with reflective surface, grey in color.

Company: Alfa Aesar

Other information: -40 + 325 mesh (0.42mm-0.04mm), 99.8% (metal basis), stock #: 00010 , Lot # A13R038

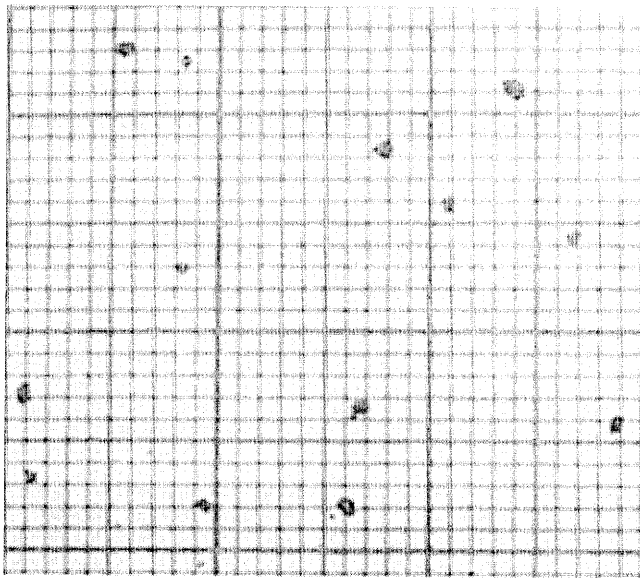


Figure above is an image of Graphite powder spread on a 1 mm. sq. grid

Material: Graphite powder, broken particles with ragged edges and dark black in color

Company: Alfa Aesar

Other information: -20 + 84 mesh (0.84mm-0.17mm) , 99% (metal basis), stock #: 1013 ,

Lot # I17PO6

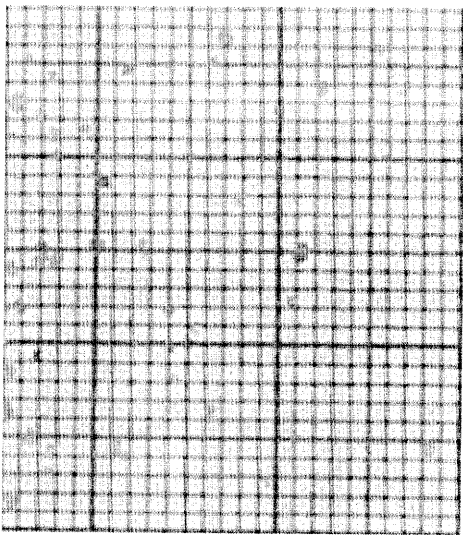


Figure above is an image of sand spread on a 1 mm. sq. grid

Material: sand, irregular in shape with different size particles and light beige in color

Company: Hartz (for pet birds)

Ingredients: Gravel, calcium (0.01%-.10%), carbonate, sorbolite clay

Other information: air washed

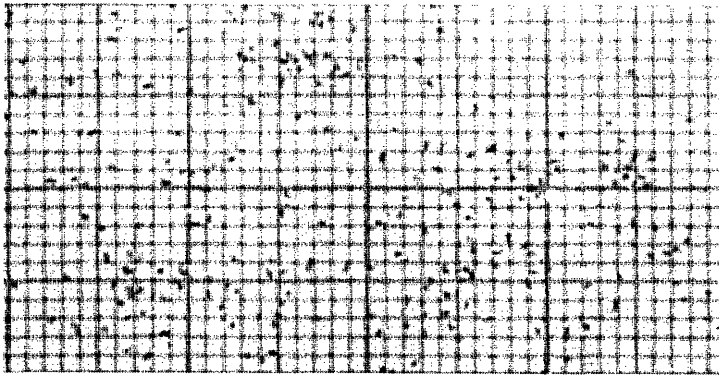


Figure above is an image of Silicon Carbide spread on a 1 mm. sq. grid

Material: Silicon Carbide, irregular shape and dark black in color

Company: McMaster Carr

Other information: 60 grit mesh (0.25mm)

B.2 Apparatus Specification

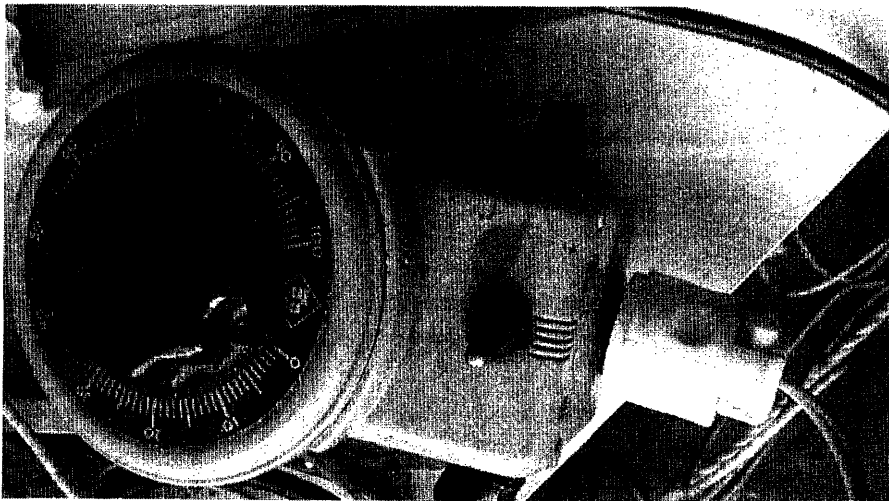


Figure above is a picture of Variac used in experimentation

Apparatus: Variac

Other information: Staco Variable Transformer 2PF751 140V/120V 7.5Amp Used

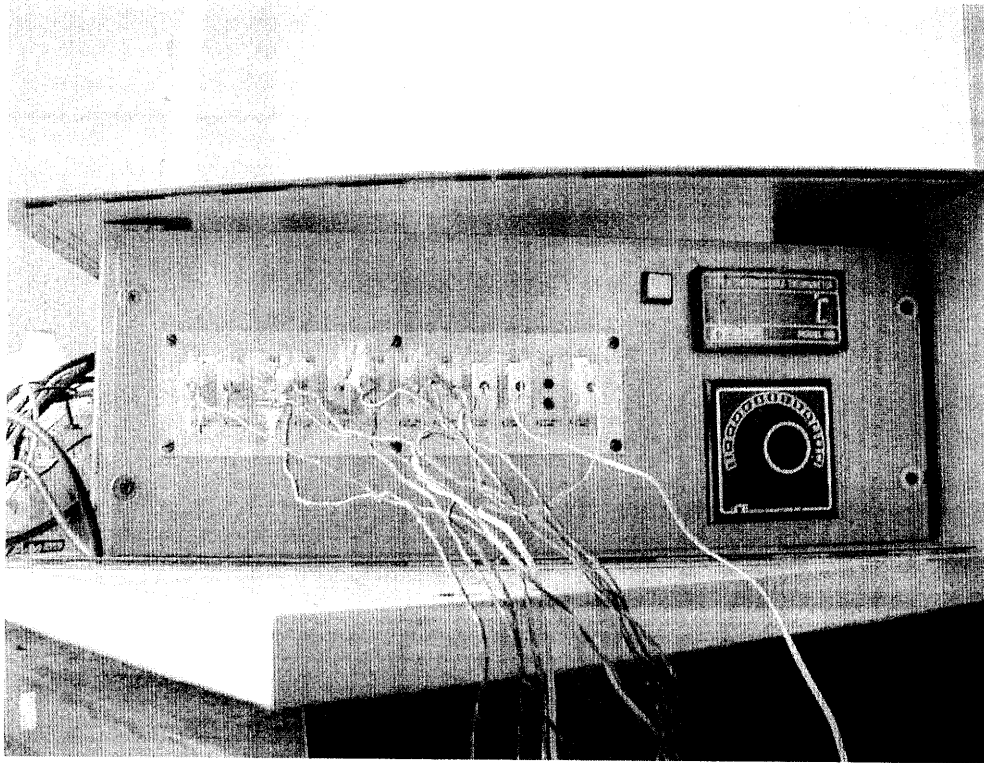


Figure above show thermocouple readout
Apparatus: Thermocouple Thermometer
Company: Omega
Other information: Model 450

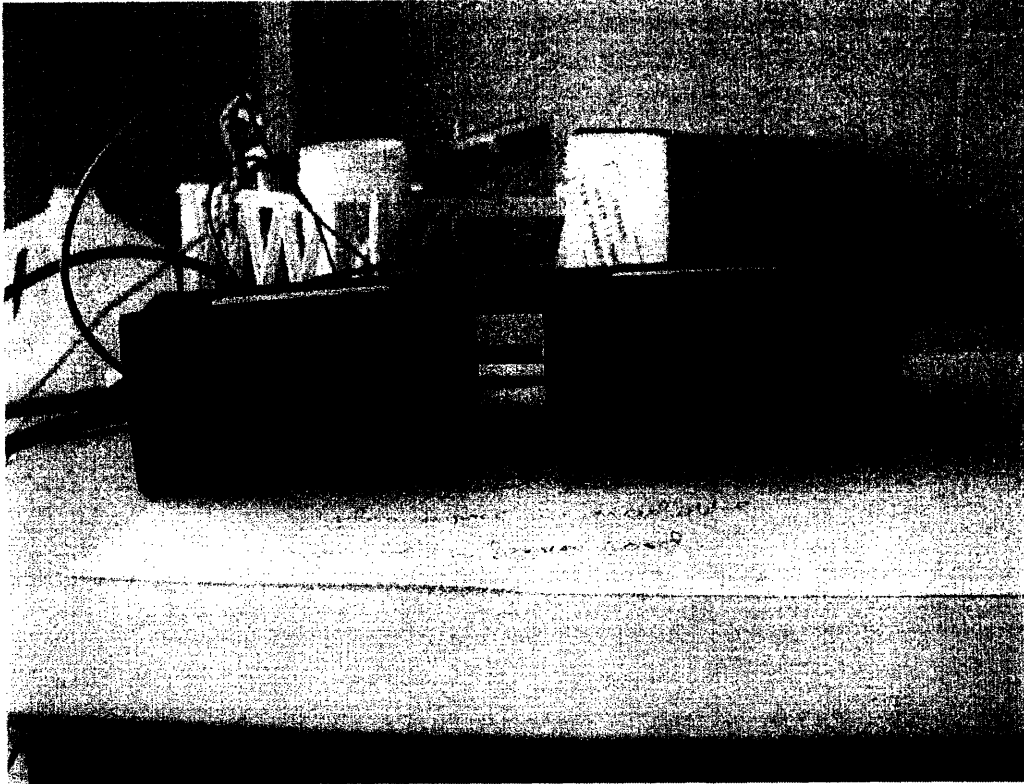


Figure above shows voltmeter and ammeter
Apparatus: voltmeter and ammeter
Company: Cole-Parmer
Other information: DP-48A, DP-48V

Appendix C: Raw Data

Data

Since there are limited outer thermocouples (those attached to the outer tube of apparatus), analysis will be limited to those thermocouples and corresponding inner thermocouples: those located on the heater.

Looking at the data the following are designated as outer thermocouple and inner thermocouples.

Inner thermocouples : #1-#8

Outer thermocouples :#9-#12

Pairing of thermocouples are as following:

2 and 12; 11 and 3; 10 and 4; 9 and 5

Analysis

In analyzing the data will average the outer thermocouples since temperature differences are relatively small. We will then be averaging corresponding inner thermocouples. The difference between the average outer thermocouple temperature and the inner thermocouple temperature will be the temperature difference used in calculating the thermal conductivity of air.

Calculations:

l (heater length): 0.47m

d (heater diameter): 0.0245m

power: ACA(value)*ACV(value)

Heater surface area ($\pi*d*l$): .0375m²

Heat flux: power/.0375m²

h: heat flux/ ΔT (average)

Date	8/8/2006
Trial #	1
Time	3:00pm
Material	grit&gravel
Variac	10%

Experimental

Run #	1
ACA	1.66
ACV	14.9
Power	24.734

Thermocouple #	Degrees in Celsius (°)
1	40
2	46
3	53
4	53
5	53
6	52
7	48
8	43
9	34
10	34
11	35
12	35

Analysis

Average Tube T	34.5
Average Heater T	51.25
ΔT (average)	16.75
Heat flux	659.5733
h	39.37751

Date	8/9/2006
Trial #	1
Time	3:30pm
Material	grit&gravel
Variac	20%

Experimental

Run #	1
ACA	3.28
ACV	29.5
Power	96.76

	Degrees in Thermoc ouple #	Celsius (°)
1	69	
2	93	
3	113	
4	115	
5	116	
6	112	
7	101	
8	85	
9	52	
10	53	
11	52	
12	52	

Analysis

Average Tube T	52.25
Average Heater T	109.25
ΔT (average)	57
Heat flux	2580.267
h	45.26784

Date	8/10/2006
Trial #	1
Time	3:30pm
Material	grit&gravel
Variac	5%

Experimental

Run #	1
ACA	0.84
ACV	7.4
Power	6.216

Degrees in Thermoc Celsius (°)	
ouple #	
1	29
2	31
3	32
4	32
5	32
6	32
7	31
8	30
9	27
10	28
11	28
12	28

Analysis

Average Tube T	27.75
Average Heater T	31.75
ΔT (average)	4
Heat flux	165.76
h	41.44

Date	7/19/2006
Trial #	1
Time	2:00pm
Material	aluminum
Variac	10%

Experimental

Run #	1
ACA	1.7
ACV	15.2
Power, W	25.84

Thermocouple #	Degrees in Celsius (°)
1	42
2	47
3	50
4	52
5	51
6	47
7	45
8	42
9	33
10	34
11	35
12	35

Analysis

Average Tube T	34.25
Average Heater T	50
ΔT (average)	15.75
Heat flux	689.0667
h	43.75026

Experimental

Run #	2
ACA	1.7
ACV	15.2
Power	25.84

	Degrees in Thermoc ouple #	Celsius (°)
1		42
2		47
3		50
4		52
5		51
6		46
7		45
8		42
9		33
10		34
11		35
12		35

Analysis

Average Tube T	34.25
Average Heater T	50
ΔT (average)	15.75
Heat flux	689.0667
h	43.75026

Date	7/20/2006
Trial #	1
Time	2:30pm
Material	aluminum
Variac	20%

Experimental

Run #	1
ACA	29.7
ACV	3.3
Power	98.01

	Degrees in Thermoc Celsius (°) ouple #
1	73
2	87
3	92
4	98
5	101
6	91
7	87
8	76
9	49
10	49
11	55
12	54

Analysis

Average Tube T	51.75
Average Heater T	94.5
ΔT (average)	42.75
Heat flux	2613.6
h	61.13684

Experimental

Run #	2
ACA	29.7
ACV	3.3
Power	98.01

	Degrees in Thermoc Celsius (°)
ouple #	
1	73
2	88
3	92
4	98
5	101
6	91
7	88
8	77
9	49
10	49
11	56
12	55

Analysis

Average Tube T	52.25
Average Heater T	94.75
ΔT (average)	42.5
Heat flux	2613.6
h	61.49647

Date	7/21/2006
Trial #	1
Time	3:00pm
Material	aluminum
Variac	5%

Experimental

Run #	1
ACA	0.92
ACV	8.2
Power	7.544

Degrees in Thermoc Celsius (°)	
ouple #	
1	29
2	30
3	30
4	30
5	30
6	29
7	29
8	28
9	26
10	26
11	27
12	27

Analysis

Average Tube T	26.5
Average Heater T	30
ΔT (average)	3.5
Heat flux	201.1733
h	57.4781

Date	8/2/2006
Trial #	1
Time	5:00pm
Material	water
Variac	10%

Experimental

Run #	1
ACA	1.63
ACV	14.6
Power	23.798

	Degrees in Thermoc Celsius (°)
couple #	
1	39
2	41
3	39
4	37
5	36
6	35
7	33
8	31
9	38
10	36
11	35
12	34

Analysis

Average Tube T	35.75
Average Heater T	38.25
ΔT (average)	2.5
Heat flux	634.6133
h	253.8453

Date	8/2/2006
Trial #	1
Time	5:00pm
Material	water
Variac	20%

Experimenta

Run #	1
ACA	3.18
ACV	28.6
Power	90.948

Thermocouple #	Degrees Celsius (°)
1	64
2	69
3	64
4	59
5	55
6	52
7	47
8	40
9	62
10	59
11	53
12	47

Analysis

Average T	55.25
Average H	61.75
ΔT (average)	6.5
Heat flux	2425.28
h	373.12

Date	8/3/2006
Trial #	1
Time	2:30pm
Material	water
Variac	5%

Experimental

Run #	1
ACA	0.88
ACV	7.8
Power	6.864

	Degrees in Thermoc ouple #	Celsius (°)
1	29	
2	30	
3	29	
4	28	
5	27	
6	27	
7	26	
8	26	
9	28	
10	28	
11	28	
12	27	

Analysis

Average Tube T	27.75
Average Heater T	28.5
ΔT (average)	0.75
Heat flux	183.04
h	244.0533

Date	6/22/2006
Trial #	1
Time	1:00 PM
Material	Air
Variac	10%

Experimental

Run #	10
ACA	1.62
ACV	14.5
Power	23.49

**Degrees in
Thermoc Celsius (°)
ouple #**

1	72
2	92
3	116
4	121
5	118
6	108
7	91
8	81
9	36
10	34
11	32
12	32

Analysis

Average Tube T	33.5
Average Heater T	111.75
ΔT (average)	78.25
Heat flux	626.4
h	8.005112

Date	6/27/2006
Trial #	2
Time	12:00pm
Material	Air
Variac	20%

Experimental

Run #	3
ACA	2.93
ACV	26.5
Power	77.645

	Degrees in Thermoc Celsius (°)
ouple #	
1	149
2	207
3	258
4	266
5	257
6	232
7	188
8	159
9	58
10	50
11	45
12	45

Analysis

Average Tube T	49.5
Average Heater T	247
ΔT (average)	197.5
Heat flux	2070.533
h	10.48371

Date	6/28/2006
Trial #	3
Time	1:00pm
Material	Air
Variac	5%

Experimental

Run #	2
ACA	0.81
ACV	7.1
Power	5.751

Degrees in Thermocouple #	
1	39
2	45
3	54
4	55
5	54
6	52
7	47
8	44
9	28
10	28
11	28
12	28

Analysis

Average Tube T	28
Average Heater T	52
ΔT (average)	24
Heat flux	153.36
h	6.39

Date	7/6/2006
Trial #	1
Time	12:30pm
Material	SiC
Variac	10%

Experimental

Run #	1
ACA	1.72
ACV	15.5
Power	26.66

Thermocouple #	Degrees in Celsius (°)
1	40
2	48
3	54
4	55
5	54
6	52
7	48
8	41
9	30
10	31
11	30
12	29

Analysis

Average Tube T	30
Average Heater T	52.75
ΔT (average)	22.75
Heat flux	710.9333
h	31.24982

Experimental

Run #	2
ACA	1.72
ACV	15.5
Power	26.66

	Degrees in Thermoc Celsius (°) ouple #
1	40
2	48
3	54
4	55
5	54
6	52
7	47
8	41
9	30
10	31
11	30
12	30

Analysis

Average Tube T	30.25
Average Heater T	52.75
ΔT (average)	22.5
Heat flux	710.9333
h	31.59704

Date	7/7/2006
Trial #	1
Time	1:30pm
Material	SiC
Variac	20%

Experimental

Run #	1
ACA	3.15
ACV	28.5
Power	89.775

Degrees in Thermoc Celsius (°)	
ouple #	
1	79
2	100
3	116
4	117
5	114
6	111
7	98
8	81
9	48
10	47
11	49
12	45

Analysis

Average Tube T	47.25
Average Heater T	111.75
ΔT (average)	64.5
Heat flux	2394
h	37.11628

Experimental

Run #	2
ACA	3.15
ACV	28.5
Power	89.775

Thermocouple #	Degrees in Celsius (°)
1	79
2	100
3	116
4	117
5	114
6	111
7	98
8	81
9	46
10	47
11	48
12	45

Analysis

Average Tube T	46.5
Average Heater T	111.75
ΔT (average)	65.25
Heat flux	2394
h	36.68966

Date	7/10/2006
Trial #	1
Time	1:30pm
Material	SiC
Variac	5%

Experimental

Run #	1
ACA	0.92
ACV	8
Power	7.36

	Degrees in Thermocouple #	Celsius (°)
1	29	
2	31	
3	32	
4	33	
5	32	
6	32	
7	31	
8	29	
9	26	
10	27	
11	27	
12	26	

Analysis

Average Tube T	26.5
Average Heater T	32
ΔT (average)	5.5
Heat flux	196.2667
h	35.68485

Experimental

Run #	2
ACA	0.92
ACV	8
Power	7.36

	Degrees in Thermoc ouple #
1	29
2	31
3	33
4	33
5	32
6	32
7	31
8	29
9	27
10	27
11	27
12	26

Analysis

Average Tube T	26.75
Average Heater T	32.25
ΔT (average)	5.5
Heat flux	196.2667
h	35.68485

Date	8/11/2006
Trial #	1
Time	5:15pm
Material	metal pipe
Variac	10%

Experimental

Run #	1
ACA	1.63
ACV	14.6
Power	23.798

	Degrees in Thermocouple #	Celsius (°)
1	58	
2	85	
3	122	
4	134	
5	132	
6	124	
7	106	
8	99	
9	31	
10	31	
11	32	
12	35	

Analysis

Average Tube T	32.25
Average Heater T	118.25
ΔT (average)	86
Heat flux	634.6133
h	7.379225

Date	8/12/2006
Trial #	1
Time	2:00 PM
Material	metal pipe
Variac	20%

Experimental

Run #	1
ACA	3.24
ACV	29.4
Power	95.256

Degrees in Thermoc Celsius (°)	
ouple #	
1	129
2	210
3	308
4	332
5	330
6	306
7	256
8	227
9	46
10	47
11	51
12	60

Analysis

Average Tube T	51
Average Heater T	295
ΔT (average)	244
Heat flux	2540.16
h	10.41049

Date	8/13/2006
Trial #	1
Time	1:30 PM
Material	metal pipe
Variac	5%

Experimental

Run #	1
ACA	1.02
ACV	8.9
Power	9.078

Degrees in Thermoc Celsius (°)	
ouple #	
1	39
2	50
3	66
4	72
5	72
6	69
7	62
8	59
9	28
10	29
11	29
12	30

Analysis

Average Tube T	29
Average Heater T	65
ΔT (average)	36
Heat flux	242.08
h	6.724444

Date	7/15/2006
Trial #	1
Time	5:40pm
Material	graphite
Variac	10%

Experimental

Run #	1
ACA	1.7
ACV	15.1
Power	25.67

Degrees in Thermoc Celsius (°) ouple #	
1	41
2	46
3	49
4	49
5	47
6	46
7	43
8	40
9	31
10	32
11	32
12	32

Analysis

Average Tube T	31.75
Average Heater T	47.75
ΔT (average)	16
Heat flux	684.5333
h	42.78333

Experimental

Run #	2
ACA	1.7
ACV	15.1
Power	25.67

Degrees in Thermoc Celsius (°) ouple #	
1	41
2	46
3	50
4	49
5	47
6	46
7	43
8	40
9	32
10	32
11	32
12	32

Analysis

Average Tube T	32
Average Heater T	48
ΔT (average)	16
Heat flux	684.5333
h	42.78333

Date	7/16/2006
Trial #	1
Time	1:00pm
Material	graphite
Variac	20%

Experimental

Run #	1
ACA	3.27
ACV	29.4
Power	96.138

	Degrees in Thermocouple #	Celsius (°)
1	83	
2	103	
3	114	
4	112	
5	108	
6	104	
7	95	
8	83	
9	52	
10	52	
11	54	
12	51	

Analysis

Average Tube T	52.25
Average Heater T	109.25
ΔT (average)	57
Heat flux	2563.68
h	44.97684

Experimental

Run #	2
ACA	3.27
ACV	29.4
Power	96.138

	Degrees in Thermoc Celsius (°)
ouple #	
1	83
2	103
3	114
4	111
5	108
6	103
7	95
8	83
9	52
10	52
11	53
12	51

Analysis

Average Tube T	52
Average Heater T	109
ΔT (average)	57
Heat flux	2563.68
h	44.97684

Date	7/17/2006
Trial #	1
Time	11:00am
Material	graphite
Variac	5%

Experimental

Run #	1
ACA	0.9
ACV	8
Power	7.2

Thermocouple #	Degrees in Celsius (°)
1	30
2	32
3	33
4	33
5	32
6	32
7	31
8	30
9	27
10	27
11	27
12	27

Analysis

Average Tube T	27
Average Heater T	32.5
ΔT (average)	5.5
Heat flux	192
h	34.90909

Experimental

Run #	2
ACA	0.9
ACV	8
Power	7.2

	Degrees in Thermocouple #
1	30
2	32
3	33
4	33
5	32
6	31
7	31
8	30
9	27
10	28
11	28
12	27

Analysis

Average Tube T	27.5
Average Heater T	32.5
ΔT (average)	5
Heat flux	192
h	38.4

References

1. Kamps, K., *The Science and Politics of the Proposed High-Level Radioactive Waste Dump at Yucca Mountain, Nevada, USA*, Nuclear Information and Resources Service, November 2003.
2. Ewing, R and MacFarlane, A. *Uncertainty Underground Yucca Mountain and the Nation's High-Level Nuclear Waste*. The MIT Press.2006
3. B. Bonin, *Deep geological disposal in argillaceous formations: studies at the Tournemire test site*, Journal of Contaminant Hydrology, Vol. 35, December 1998, 315-330.
4. Hoag, I. *Canister Design for Deep Borehole Disposal of Nuclear Waste*. SM thesis Dept. of Nuclear Eng. Massachusetts Institute of Technology. 2006.
5. *Safety and Security of Commercial Spent Nuclear Fuel Storage: Public Report (2006)* Board on Radioactive Waste Management
6. Hall, R.O.A, Martin, D.G, *The Thermal Conductivity of Power Beds. A Model, Some Measurements on UO₂ Vibro-Compacted Microspheres, and Their Correlation*, Journal of Nuclear Materials 101 (1981) 172-183.
7. G.K. Batchelor and R.W. O'Brien "Thermal or Electric Conduction Through a Granular Material" Proc. R. Soc. London, A, Vol. 355, No 1682, p 313, 13 July 1977
8. Cho, Y, Hartnett, J., and Rohsenow, W., *Handbook of Heat Transfer*. McGraw-Hill. 1998.
9. Mikheyev, M., *Fundamentals of Heat Transfer*. Peace Publishers. 1977, p 83-85, .
10. Callister, William (2003). "Appendix B", *Materials Science and Engineering - An Introduction*. John Wiley & Sons, Inc., 757. [ISBN 0-471-22471-5](#).
11. McAdams, W.H., *Heat transmission*. McGraw-Hill Book Company. 1954.
12. Gokel, G. *Dean's Handbook of Organic Chemistry*. McGraw-Hill Professional; 2 edition (2003).
13. Lide, D. *CRC Handbook of Chemistry and Physics*, 87th Edition. CRC; (2006)
14. Kuo, W.S., "Evaluation of Deep Drillholes for High Level Nuclear Waste Disposal," Eng. Thesis MIT Dept. of Nuclear Eng. Massachusetts Institute of Technology, 1981.

15. Novak, J. Conception and Experimental Investigation of Thermal Switches. SM thesis MIT Nuclear Eng. Dept. Massachusetts Institute of Technology. 1995.
16. Marques, A. CANDU Pressure/ Calandria Tube Emergency Water Injection System. SM thesis MIT Nuclear Eng. Thesis. Massachusetts Institute of Technology. 1998.
17. Manteufel, R.D., and Todreas, N.E., "Effective Thermal Conductivity and Edge Conductance Model for a Spent-Fuel Assembly," Nuclear Technology, Vol. 105, 1994.
18. Hall, R.O.A, and Martin, D.G., and Mortimer, M.J., "The Thermal Conductivities of UO₂ Sphere-Pac Beds", Journal of Nuclear Materials, Vol. 173, 1990.



Room 14-0551
77 Massachusetts Avenue
Cambridge, MA 02139
Ph: 617.253.5668 Fax: 617.253.1690
Email: docs@mit.edu
<http://libraries.mit.edu/docs>

DISCLAIMER OF QUALITY

Due to the condition of the original material, there are unavoidable flaws in this reproduction. We have made every effort possible to provide you with the best copy available. If you are dissatisfied with this product and find it unusable, please contact Document Services as soon as possible.

Thank you.